

Review

Applications of Fluorescent Carbon Dots as Photocatalysts: A Review

Ricardo M. S. Sendão¹, Joaquim C. G. Esteves da Silva^{1,2}  and Luís Pinto da Silva^{1,2,*} 

¹ Chemistry Research Unit (CIQUP), Institute of Molecular Sciences (IMS), Department of Geosciences, Environment and Territorial Planning, Faculty of Sciences (FCUP), University of Porto, Rua do Campo Alegre s/n, 4169-007 Porto, Portugal

² LACOMEPI, GreenUPorto, Department of Geosciences, Environment and Territorial Planning, Faculty of Sciences (FCUP), University of Porto, Rua do Campo Alegre s/n, 4169-007 Porto, Portugal

* Correspondence: luis.silva@fc.up.pt

Abstract: Carbon dots (CDs) have attracted considerable interest from the scientific community due to their exceptional properties, such as high photoluminescence, broadband absorption, low toxicity, water solubility and (photo)chemical stability. As a result, they have been applied in several fields, such as sensing, bioimaging, artificial lighting and catalysis. In particular, CDs may act as sole photocatalysts or as part of photocatalytic nanocomposites. This study aims to provide a comprehensive review on the use of CDs as sole photocatalysts in the areas of hydrogen production via water splitting, photodegradation of organic pollutants and photoreduction and metal removal from wastewaters. Furthermore, key limitations preventing a wider use of CDs as photocatalysts are pointed out. It is our hope that this review will serve as a basis on which researchers may find useful information to develop sustainable methodologies for the synthesis and use of photocatalytic CDs.

Keywords: carbon dots; photocatalysis; hydrogen generation; photodegradation; photoreduction



Citation: Sendão, R.M.S.; Esteves da Silva, J.C.G.; Pinto da Silva, L. Applications of Fluorescent Carbon Dots as Photocatalysts: A Review. *Catalysts* **2023**, *13*, 179. <https://doi.org/10.3390/catal13010179>

Academic Editors: Amr Fouda and Mohammed F. Hamza

Received: 12 December 2022

Revised: 4 January 2023

Accepted: 6 January 2023

Published: 12 January 2023



Copyright: © 2023 by the authors. Licensee MDPI, Basel, Switzerland. This article is an open access article distributed under the terms and conditions of the Creative Commons Attribution (CC BY) license (<https://creativecommons.org/licenses/by/4.0/>).

1. Introduction

In recent years, nanostructured materials have arisen as potential substitutes for traditional materials due to the unique properties and functionality enabled by their nanosized composition. Carbon nanomaterials have been studied for applications in diverse fields, one of them being photocatalysis, a process through which radiation is used to promote a chemical reaction without consuming the photocatalyst. Carbon is a black material that, when in bulk, is non-soluble in water and incapable of displaying photoluminescence. However, this is not true for carbon-based nanomaterials, which display properties that greatly differ from those of the bulk material [1–4]. These carbon-based nanomaterials include single and multi-wall carbon nanotubes [1–3], nanofibers [4], nanodiamonds [5], graphene [6], buckminsterfullerene [7] and, more recently, CDs. First discovered in 2004 by Xu et al. [2] during the synthesis of single-wall carbon nanotubes, CDs are a class of carbon nanomaterials that gained their name in 2006 from Sun et al. [8] and have been under the focus of the scientific community ever since.

As seen in Figure 1, CDs display a spherical or quasi-spherical shape with a sp^2 -conjugated amorphous or nanocrystalline core and are typically sized between 1 and 10 nm, depending on the synthesis. Whereas oxygenated functional groups can be found on the surface (e.g., -OH, -COOH and CHO) [9,10], CDs' cores are mostly composed by sp^2 carbon or graphene/graphene oxide sheets connected by sp^3 carbon atoms in-between [11,12]. The CDs' surface may present several functional groups (e.g., alcohols, amines and carboxylic acids) that contribute towards the CDs superior water solubility while also allowing the CDs to undergo additional steps of functionalization by providing a binding site for other molecules if needed [11]. The result from this, and considering that the CDs' core type can also be controlled during the synthesis, is that these nanoparticles present a complex

internal and external structure, whose constitution is highly dependent on the precursors and synthetic conditions [13].

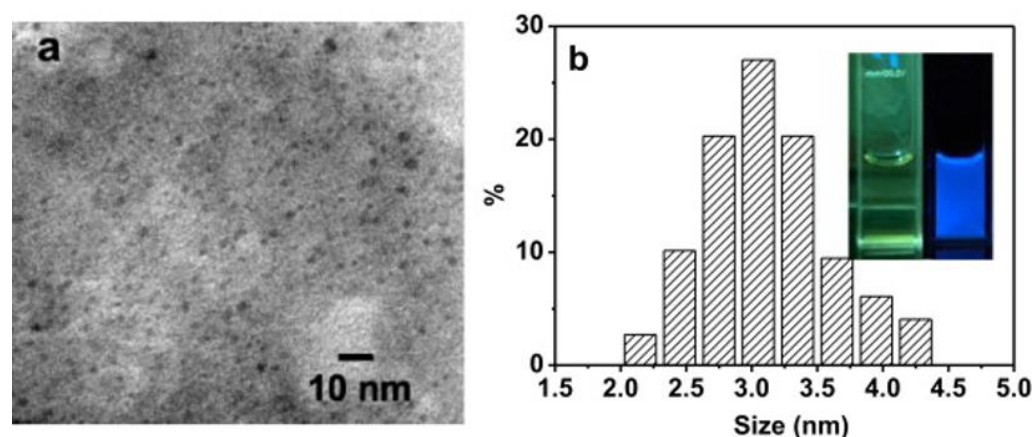


Figure 1. (a) TEM image of plant soot-derived CDs; (b) size distribution of the CDs determined by measuring 150 CDs via TEM. Reproduced with authorization from [14].

Depending on the chosen method, the synthesis of CDs can be divided into two categories: top-down and bottom-up approaches (Figure 2). Synthesis via top-down methodologies is based on breaking macroscopic carbon-based materials (e.g., graphite or activated carbon) into smaller nanosized particles, the CDs. This can be achieved using methods such as arc discharge [2], laser ablation [8], chemical [15] and electrochemical oxidation [16], and ultrasonic synthesis [17]. On the other hand, we have the bottom-up approach, which is based on the fabrication of CDs from molecular components, such as citric acid. This can be conducted via microwave treatment [18], thermal decomposition [19], hydrothermal treatment [20], template-based routes [21] and plasma treatment [22]. Due to the low cost and relative easiness of the preparation in some methods, the fabrication of CDs is possible in virtually any environment without requiring expensive and time-consuming techniques.

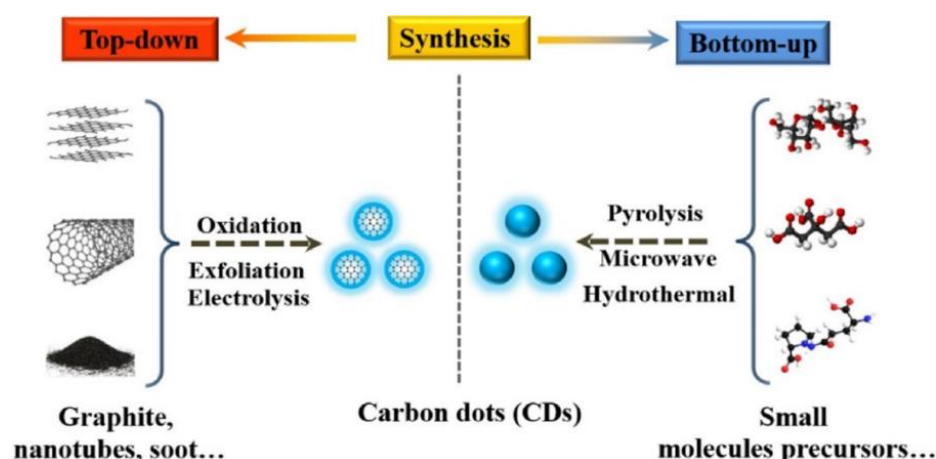


Figure 2. Top-down and bottom-up synthetic pathways for CDs. Reproduced with authorization from [23].

One of the reasons behind the interest in CDs is their many desirable properties, such as high photoluminescence (PL) [9,24], broadband optical absorption and large photore sponsive region [25], high photo- and chemical stability [26], good water solubility [9,26], biocompatibility [8,27] and low toxicity [28]. It is also possible to fabricate CDs with up-conversion PL (UCPL), which can convert lower-energy higher-wavelength radiation into higher-energy lower-wavelength radiation, which is useful for photocatalytic nanocomposites [29]. Characterization of the CDs properties is usually performed using methods

such as TEM/SEM (Figure 1), UV-Vis and fluorescence spectroscopy (Figure 3a), FTIR (Figure 3b) and XPS (Figure 3c), among others.

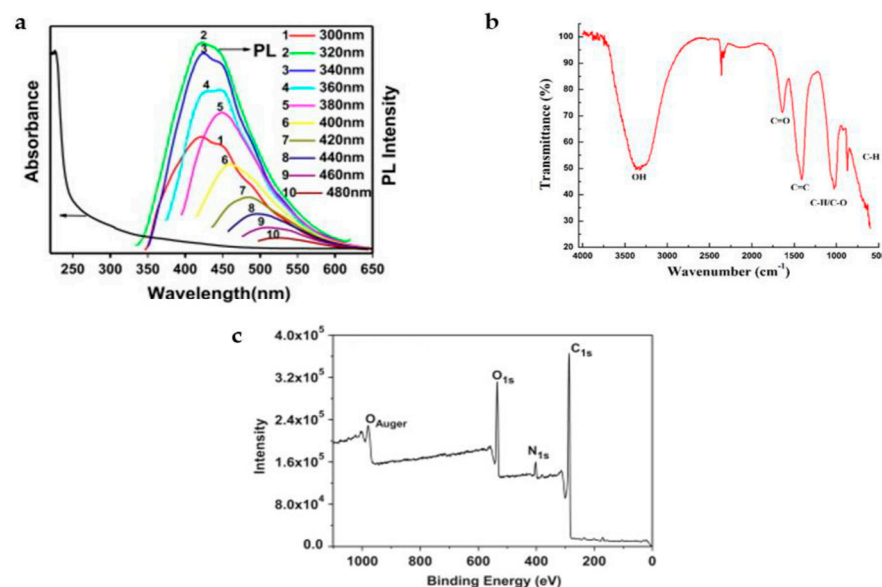


Figure 3. (a) UV-Vis absorption spectrum (left) and photoluminescent emission spectra of plant soot-based CDs at several excitation wavelengths; (b) FTIR spectrum of Fennel seeds-based CDs; (c) XPS spectrum of plant soot-based CDs. Reproduced with authorization from [14,30].

Photocatalysis refers to the conversion of materials induced by a synergistic effect between photocatalysts and light. It aims to accelerate reactions, such as the generation of hydrogen from water [31,32] or the photodegradation of organic pollutants (e.g., azo dyes) [33,34], consisting of an environmentally-friendlier technology when compared to traditional catalysts [35]. The critical step in the process is the light-induced separation of charge carriers, with an ideal photocatalyst presenting both a broad absorption range and a high separation efficiency of the photogenerated charge carriers [36]. This charge separation depends on the absorption, by the CDs, of light with enough energy to overcome the nanoparticles' energy bandgap [37]. Several factors might impact a CD energy bandgap. The CDs' structure configuration impacts the bandgap [38,39]. The size of the CDs is also an important factor, and it is known that larger nanoparticles present a smaller bandgap [38,39]. Finally, doping with heteroatoms and higher degrees of surface functionalization on the CDs can be used to decrease the energy bandgap [40–42].

CDs are able to photogenerate charge carriers upon the absorption of light. Furthermore, the highly functionalized surface of the CDs provides adsorption spots for organic compounds, such as organic dyes. This promotes the photocatalytic reaction, as the reaction takes place on the CDs' surface and there is less energy wasted due to charge recombination (that could occur due to the small band gap presented by CDs). Due to this and considering the properties of CDs, it is not surprising that their use in photocatalytic applications has been reported, with the nanoparticles being used in roles such as electron mediators [43–45], photosensitizers [46–48], spectral converters [49–51] and, finally, as a sole photocatalyst [31–34,52–57]. Whereas this review focuses on the use of CDs in photocatalysis, the use of CDs in photocatalytic nanocomposites is not under the scope of this study. More specifically, we focused only on cases in which CDs were used as sole photocatalysts without any additional component. We intend to provide a basis where researchers may find useful information for future developments of CDs as sole photocatalysts.

2. Application as Sole Photocatalysts

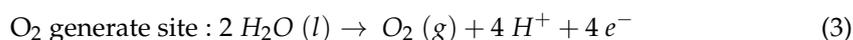
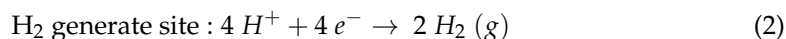
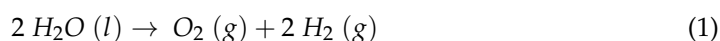
Regarding photocatalysis, CDs have already been employed in several roles. Despite this, the use of CDs as sole photocatalysts is somewhat rare, and thus worthy of a detailed

analysis. Thus far, they have been mainly used in the fields of hydrogen production via water splitting [31,58–60], photocatalytic degradation of organic compounds [33,54,57,61] and photoreduction [52,53,55,56].

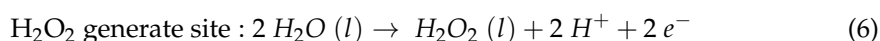
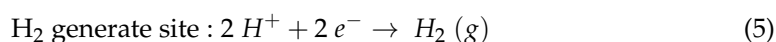
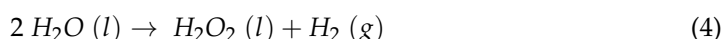
2.1. Hydrogen Generation via Water Splitting

The use of hydrogen as an energy source is a cleaner alternative to evermore depleted fossil fuels. First discovered by Fujishima and Honda in 1972 [62], hydrogen production via solar-driven photocatalytic water splitting has been vastly studied as a green pathway for the obtention of H₂ to cover our energy requirements. Thus, it is not surprising that there is a strong demand for a renewable energy source of this kind. H₂ is regarded as an optimal energy carrier due to being environmentally friendly, carbon-free and renewable, all of this while also having a high energy density. The generation of H₂ via water splitting has been under the spotlight, as H₂O, the initial reagent, is the only product after H₂ combustion, thus enabling a cyclic use of the fuel [63]. Near 237 kJ mol⁻¹ of energy is required to produce H₂ and O₂, being the overall process endothermic. That being said, the bandgap of a suitable photocatalyst must be in a way that its conduction band is more negative than the redox potential of H⁺/H₂, which sits at 0 V vs. NHE, and the valence band should be more positive than the potential of O₂/H₂O, 1.23 V vs. NHE. Hence, the smallest possible bandgap required for the reaction is 1100 nm, which corresponds to the 1.23 V difference between the reactions [64]. The water splitting reaction is made of two half-reactions: the H₂ evolution reaction (HER) and the O₂ evolution reaction (OER).

The typical four electron half-reactions are as follows:



While the two-step 2e⁻/2e⁻ first generates H₂ and H₂O₂ from water, followed by the release of energy due to the disproportionation of H₂O₂:



There is a multitude of photocatalysts capable of H₂- and O₂-evolution via water splitting under irradiation. The photocatalytic mechanism, as seen in Figure 4, begins when under a suitable light source, the photocatalyst's electrons are excited into the conduction band, leaving behind holes in the valence band. Then, the newly generated electron/hole pairs transfer to the photocatalyst's surface, with the electrons moving to the H₂ generation sites and the holes to the O₂ generation sites. Because of this, and due to their properties (such as a large photoresponsive absorbing region and a convenient bandgap for HER), CDs are now used for photocatalytic H₂ evolution in aqueous solutions, being regarded as an effective way of broadening the light-range on which the reaction takes place into the visible [48].

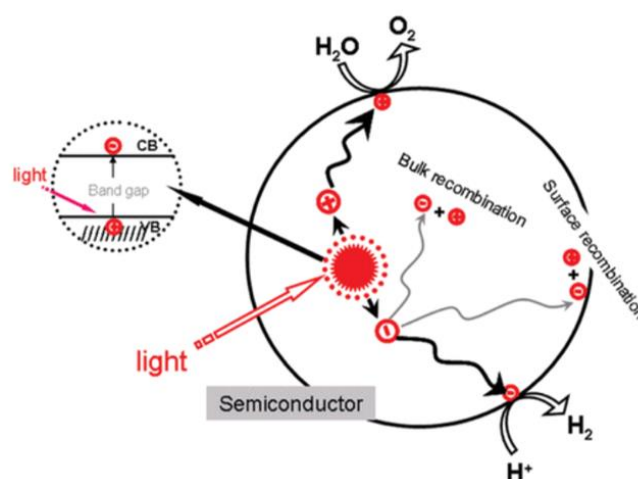


Figure 4. Representation of photocatalytic water splitting with semiconductors. Reprinted with permission from [65]. Copyright 2010 American Chemical Society.

Regarding hydrogen evolution via water splitting, CDs are mostly used in conjunction with other components, such as NiP and TiO₂ [46,48], to obtain a photocatalytic nanocomposite, seldom being used as sole photocatalysts. However, in the last few years, development of CDs has been a constant trend, and some teams already achieved H₂ evolution using CDs as the sole photocatalytic agent [31,32,59,60,66,67].

In this regard, Yang et al. reported the preparation of glucose-based CDs via light irradiation for both the detection of Fe³⁺ and the photocatalytic production of hydrogen under Xe lamp irradiation [32]. Upon characterization, the CDs were observed to present homogeneous sizes and displayed a typical CD absorption spectrum with broadband absorption, ranging from the UV to the NIR. FTIR and XPS experiments confirmed the presence of the expected C=C, C-OH, C-O-C and C-H groups on the CDs surface, whereas Raman spectroscopy confirmed the presence of sp² and sp³ carbon atoms on its core [32]. The photocatalytic H₂ production was tested using both the CDs alone and in conjunction with a Pt co-catalyst, under a 300 W Xe lamp. The team estimated hydrogen evolution rates as high as 1.004 and 2.329 mmol g⁻¹ h⁻¹ for the CD alone and with a Pt co-catalyst, respectively [32]. Despite the fact that with Pt the rate is over twice that of the CDs alone, it is still important to notice that a non-metallic, inexpensive and low toxicity photocatalyst was able to produce H₂ by itself [32].

In another example, Yang et al. prepared photocatalytic CDs via an ultrasonic hydrothermal procedure from multi-walled carbon nanotube oxide to promote hydrogen generation through water splitting [66]. As in the previously mentioned work [32], the CDs present an oxygenated surface (with groups such as C-O-C, C=O and C-OH) and a characteristic broadband absorption [66]. The photocatalytic hydrogen generation under UV radiation, in pure water and in without any sacrificial agent, reached 423.7 μmol g⁻¹ h⁻¹, which is below half of that achieved in [32], whereas by employing methanol as a sacrificial donor (20 vol%) the rate reached 3615.3 μmol g⁻¹ h⁻¹, over 8.5 times that of the CDs alone [66]. Furthermore, when compared to commercial Degussa P25 TiO₂, the CDs present a higher hydrogen generation rate both in the absence (423.7 vs. 16.25 μmol g⁻¹ h⁻¹) and presence of methanol (3615.3 vs. 103.7 μmol g⁻¹ h⁻¹) as a sacrificial donor. Control tests in the absence of either CDs or UV light irradiation failed to yield any hydrogen, indicating that its production is the result of a photocatalytic process involving the CDs. Finally, the CDs stability as a photocatalyst was tested, and its reusability confirmed, as the HER had negligible changes after four cycles of testing [66].

A final example regarding the evolution of HER with CDs is the 2021 work of Jana et al. [59], which describes the making of a modified CD, from citric acid and urea, that allowed for an efficient hydrogen production from both water and seawater via water splitting. The CDs were prepared by subjecting the precursors to microwave irradiation

under pressure (15 bar) for 5 min, followed by purification via dialysis (MWCO 1000 Da, 24 h) and evaporation of the solvent. Afterwards, the resulting solid nanoparticles (pCD) were subjected to a post-synthetic photo-oxidation treatment. This consisted of white light irradiation in the presence of oxygen and took place until absorption peaks at 600 and 450 nm were maximized, yielding two different activated CDs (CD1 and CD2, the latter being the result of a more prolonged exposure) [59].

Upon characterization, the three types of CDs appear to be similar in terms of shape and size, presenting an amorphous body sized between 2.5 and 3.5 nm, as seen by AFM and XRD. However, their fluorescence peaks differ when excited at 350 nm, with CD2 showing a red-shifted emission (500 nm) compared to pCD and CD1 (440 nm). The quantum yields also decrease in function of the irradiation time, going from 12% for the pCDs to 2% for CD2 [59]. It should be noted that lower quantum yields have been correlated with increased HER activity in similar materials [68]. Cyclic voltammetry tests show that, based on their electrocatalytic proton reduction potentials, all CDs are active HER electrocatalysts. More importantly for our review, tests using methyl viologen demonstrate the potential of pCDs, CD1 and CD2 for HER photocatalysis, with CD2 being the most active photocatalyst in the presence of sacrificial electron donors [59].

Regarding the efficiency of the HER reaction itself, it was evaluated with optimal conditions being found to be 0.015 mg of catalyst, pH of 8.5 and a 10 vol% solution of the sacrificial donor triethanolamine (TEOA) [59]. Control experiments revealed that in absence of CDs, TEOA produces small amounts of H₂, so this was taken into consideration in all subsequent experiments. Regarding HER catalysis, CD2 was the most effective, achieving a maximum turnover frequency (TOF) of 15.15 mmol (H₂) g(CD2)⁻¹ h⁻¹ after 1 h of Xe lamp illumination in water and 19.70 in seawater [59]. The different TOF may be explained by the different ionic strength of the two media, which might impact electron transfer rates. As for their stability, whereas pCD and CD1 appear to remain relatively unchanged after the reaction, CD2 shows a different spectral profile, suggesting some degree of degradation or modification after the catalysis, possibly due to TEOA [59]. Finally, when assessing the mechanism behind the catalysis, the team found that one of the components produced during the CDs synthesis, citrazinic acid, could be responsible for the enhanced catalytic activity of the CDs [59]. Thus, some further characterization of the system should be performed to better understand the photocatalytic mechanism.

2.2. Photocatalytic Degradation of Organic Pollutants

The continuous development of manufacturing methods by mankind has improved the quality of life found around our planet. However, it has also led to the production of new potential pollutants, causing the number of chemicals known to be in circulation (in 2011) to be nearly 38,000, with an estimated 300 new compounds being added to the list each year [69,70]. Tons of domestic and industrial pollutants enter the waterways daily, being harmful not only to human health, but also to the environment and surrounding ecosystems [71,72]. As a result of this, we find ourselves with an ever-smaller unpolluted supply of drinkable water [73,74]. Common causes of water pollution that need to be addressed are industrial effluents, heavy metals (e.g., cadmium and chromium) and organic compounds. The latter, and the focus of this section, can consist of either small organic compounds (such as drugs or dyes) or longer chained molecules (such as perfluorooctane sulfonate or perfluorooctanoic acid). This prompts the need for obtaining efficient and cost-effective means for their removal after they have been used, discarded or lost their functionality. Several alternatives are available for use nowadays, including photocatalytic technologies that take advantage of a renewable energy supply and sunlight, to eliminate these pollutants [75].

Photocatalytic degradation is a process through which a photocatalyst, upon absorption of suitable radiation, can transform a pollutant adsorbed onto its surface into a less harmful degradation product. Photocatalysis has several advantages over traditional chemical oxidation, such as being environmentally friendlier, achieving a near complete

degradation of the pollutants, and not originating any by-products from the photocatalyst during the reaction [35]. In typical photocatalytic degradation (Figure 5), a semiconductor absorbs suitable radiation to overcome its bandgap, which excites an electron (e^-) from the valence band into the conduction band, leaving behind an electron–hole (h^+). The photo-generated e^- and h^+ are photoreactive and can cause a cascade of reactions that end in the degradation of the pollutants by converting them into CO_2 and H_2O . Thus, using photocatalysts enables us to convert solar energy into a chemical reaction that degrades a pollutant into a benign/less harmful form [76]. This process is however severely limited by a rapid recombination of the photogenerated charge carriers, which can release energy as heat or radiation. The latter consists of a phenomenon known as photoluminescence, a property which CDs are known to possess. However, it is a competing process to photodegradation itself, and might lead to a decay in its efficiency.

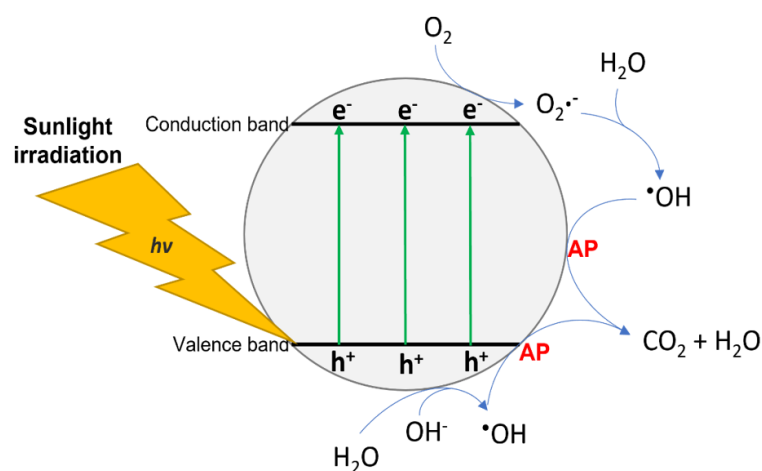


Figure 5. General photocatalytic degradation mechanism. AP—adsorbed pollutant. Represented here with authorization from [75].

The use of CDs or CDs-composites for the photodegradation of organic pollutant has been a widely developed field over the last decade. They have been employed, both as sole photocatalysts and in conjugation with other materials (such as TiO_2), to degrade a vast array of organic pollutants, ranging from organic dyes to antibiotics [33,57,77–86]. Properties commonly associated with CDs, such as their tunable structure and functionalized surface (providing affinity to organic compounds), low-cost, water solubility, non-metallic and non-toxic nature, (photo)chemical stability, and strong absorption across the light spectrum, makes these nanoparticles potentially viable candidates to be employed in photocatalysis. While these properties benefit both the use of CDs as parts of catalytic systems and as sole photocatalysts, this review focuses only on the latter.

Despite the large advances achieved in the synthesis of CDs, photocatalysis and photocatalytic removal of pollutants, there are still very few reports where CDs were directly used as the photocatalytic agent. However, the number of such reports is continuously growing as the scientific community becomes more interested in the potential of CDs. One of the first reports concerning this topic came from Umrao et al., who achieved the photodegradation of methylene blue (MB), under blue and green light, by using multilayered CDs from graphene oxide via a hydrothermal method [77]. The resulting CDs showed a high degree of crystallinity and an average size of 9 nm. They presented the typical C-C, C=O, C-OH and COOH groups on their surface and displayed an absorption that extends well into the visible range [77]. A degradation efficiency of 93.3% was observed under 60 mins of green light irradiation with a rate constant of 0.056 min^{-1} , which was ~ 17 times higher than bare TiO_2 (0.0033 min^{-1}) [77,87]. In another example, Zhu et al. prepared xylose-based CDs that achieved 92.06% photodegradation of MB within 2.5 mins of Xe lamp irradiation [54].

Zhou et al. fabricated gel-like CDs from citric acid and ethylenediamine, and used them under solar light irradiation to photodegrade several common organic dyes [57]. The CDs managed to degrade all the tested pollutants, MB, methyl orange (MO) and rhodamine B (RhB), in 20, 40 and 60 mins, respectively [57]. Several other examples can be found for varied organic dyes, such as MB [33,34,78,88–93], RhB [33,78,89,93], MO [61,94,95], crystal violet (CV) [84,96], indigo carmine (IC) [79,85], methyl violet [95], metanil yellow (MY) [61] and malachite green (MG) [95]. A list can be found below, in Table 1, containing a summary of several studies concerning the topic.

Table 1. Summary of studies concerning CDs’ mediation photodegradation of organic pollutants. NA—not available; CFL—compact fluorescent lamp.

| Ref. | CDs’ Precursors | Synthesis/Purification | CDs Loading | Pollutant/Concentration | Light Source/Power | Dye Removal Efficiency and Time |
|------|--|---|----------------------|---|---|---|
| [77] | Graphene | Hydrothermal/Centrifugation | NA | MB-83 mg L ⁻¹ | LED (520 nm) 1 W/mm ² | 93.3%/60 mins |
| [54] | Xylose | Hydrothermal/Filtering Dialysis | 30 mg | MB-1 g L ⁻¹ | Xe lamp 150 mW/cm ² | 92.06%/2.5 mins |
| [57] | Citric acid Urea | Solvothermal/Acetone wash | 12 mg | MB-10 mg L ⁻¹ MO-10 mg L ⁻¹ RhB-10 mg L ⁻¹ | Hg/Xe lamp | 100%/20 mins 100%/40 mins 100%/60 mins |
| [93] | Pyrene | Hydrothermal/Filtering Dialysis | 0.3 mg | RhB-10 mg L ⁻¹ MB-10 mg L ⁻¹ | LED and CFL Flux of 1000 lm | 55%/360 mins 39%/360 mins |
| [34] | Citric acid 1,2-phenylenediamine | Microwave/Filtration Chromatography | 3 mg | RhB-0.5 mg L ⁻¹ MB-2.5 mg L ⁻¹ | Hg/Xe lamp 310 W | 100%/150 mins 100%/150 mins |
| [78] | Palm powder Thionyl chloride | Hydrothermal/Filtering Dialysis | NA-added in solution | MB-15 mg L ⁻¹ RhB-15 mg L ⁻¹ | Xe lamp 400 mW/cm ² | 94.2%/50 mins 71.7%/50 mins |
| [88] | Glucose Ethylenediamine Phosphoric acid | Microwave/Centrifugation Dialysis | 2 mg | MB-10 mg L ⁻¹ | Sunlight ~832 W/m ² | 100%/25 mins |
| [89] | Citric acid 1,2-diboranyethane Dimethylformamide | Hydrothermal/Centrifugation Dialysis | 3 mg | MB-2.5 mg L ⁻¹ RhB-0.5 mg L ⁻¹ | Hg/Xe lamp 310 W | 100%/170 mins 100%/170 mins |
| [90] | Citric acid Hexamethylene-1,6-diamine | Hydrothermal/Centrifugation Dialysis | 10 mg | MB-5 µM | Xe lamp 110 mW/cm ⁻² | 96.7%/40 mins |
| [91] | Pear juice | Hydrothermal/Filteration | NA-added in solution | MB-45 µM | Tungsten lamp 60 W | 99.5%/130 mins |
| [92] | Citric acid Diethylenetriamine | Hydrothermal None | 0.2 mg | MB-18.75 mg L ⁻¹ | Sunlight and Halogen lamp (500 W) | 97%/160 mins |
| [61] | Polyethylene glycol Phosphoric acid Cysteine | Microwave/Dialysis | 25 mg | MO-20 mg L ⁻¹ MY-20 mg L ⁻¹ | Sunlight | 100%/90 mins 100%/60 mins |
| [94] | Glucose Ammonia | Ultrasonic treatment/Dialysis | NA-added in solution | MO-10 ppm | Xe lamp 150 W | 90%/120 mins |
| [95] | <i>Cornus walteri</i> leaves Malei anhydride Hydrogen peroxide | Hydrothermal/Centrifugation Filtration Dialysis | 1 mg | MO-30 mg L ⁻¹ MG-30 mg L ⁻¹ MV- 30 mg L ⁻¹ | Sunlight | 97.1%/50 mins 98.0%/40 mins 63.6%/60 mins |
| [84] | Bitter apple peel | Calcination/ None | 10 mg | CV-200 ppm | Sunlight | 100%/90 mins |
| [79] | 2-aminonaphthalene Potassium persulfate | Hydrothermal/Centrifugation Dialysis | NA-added in solution | IC-10 mg L ⁻¹ | Natural light | 97%/120 mins |
| [85] | Glyoxal Ethanol | Solvothermal None | 0.265 mg | IC-38.8 mg L ⁻¹ | Sunlight | 91%/4.5 mins |

Heteroatom doping is a process through which the optical properties of CDs, such as PL, can be improved. The presence of nitrogen and oxygen atoms in the structure of the CDs could cause an upward band bending electric field near their surface, and thus spatially separate the photogenerated e^- - h^+ pair and reduce the rate of recombination, promoting h^+ and e^- to the surface, where they can generate ROS [36,97]. Furthermore, tuning the surface charge of the CDs via doping, such as is the case with N-doping, might promote the adsorption of organic pollutants, based on their own charge, via electrostatic interactions [93]. This being said, N-doped CDs have been synthesized and employed in organic pollutant photodegradation. The work of Sabet et al., who fabricated photocatalytic N-doped CDs via hydrothermal treatment from a green carbon source, grass, is a great example of this and of the versatility of the CDs in terms of degradation targets [98]. The CDs were effectively used for the UV-light-driven photodegradation of four different dyes, which showcases their versatility in the field of pollutant photodegradation. When characterized, the nanoparticles were revealed to be under 10 nm in size, to be effectively N-doped (as seen by EDS) and to present all the common surface functional groups, in addition to N-H, on their surface. The nanoparticles were capable of absorbing both UV and visible radiation, thus increasing their photocatalytic region [98]. Results from photocatalytic tests demonstrated the CDs' efficiency in decomposing the selected dyes, and that the degradation was due to the production of ROS in aqueous medium by the CDs. Regarding the individual results for each dye under UV irradiation: acid blue and acid red were completely degraded after 30 mins whereas eosin Y and MB were fully decomposed after 90 mins. The authors state that the CDs also worked under visible light irradiation, but no data has been provided regarding this [98]. In another example of N-doped CDs, Aghamali et al. described the making of citric acid and diethylenetriamine-based N-doped CDs for the photocatalytic degradation of MB [92]. The hydrothermally-prepared CDs displayed a spherical shape with an average size of 4.5 nm, an impressive quantum yield of 95%, and presented the functional groups expected on a N-doped CD (including C-N and N-H, in addition to oxygen-based groups) [92]. The authors evaluated the photocatalytic efficiency of the CDs towards MB degradation under sunlight, UV and visible irradiation. When exposed to sunlight/visible light, the photodegradation efficiency was very high, as the CDs achieved nearly complete degradation of MB (97%), which was the best catalytic performance obtained. These results suggest that the N-doped CDs may be an efficient visible and sunlight-driven photocatalyst [92].

Other kinds of doping and combinations thereof can also be employed to enhance the CDs' optical properties, and thus, their photocatalytic efficiency. Peng et al. synthesized boron-doped CDs towards the photocatalytic degradation of RhB and MB [89]. Their CDs were made from citric acid, 1,2-diboranyethane and dimethylformamide via a hydrothermal method. In terms of photocatalytic efficiency, the CDs achieved complete degradation of both RhB and MB within 170 mins under solar light irradiation [89]. Zhu et al. made N,Cl-doped CDs out of palm powder and thionyl chloride via hydrothermal treatment [78]. The CDs displayed good photocatalytic efficiency, degrading 71.7 and 94.2% of the initial concentrations of RhB and MB within 45 mins of visible light irradiation [78]. Yashwanth et al. fabricated N,P-doped CDs from glucose, phosphoric acid and ethylenediamine via a microwave-assisted methodology [88]. The CDs completely photodegraded MB within 25 mins of visible light irradiation [88]. Saini et al. prepared N,S,P-doped CDs from polyethylene glycol, phosphoric acid and cysteine via a microwave charring process [61]. The CDs were effective in removing both metanil yellow and methyl orange under sunlight irradiation [61].

Several parameters and properties affect the photocatalytic potential of the CDs. To study this, Ibarbia et al. compared the effect that different types of CDs have on the photodegradation efficiency of organic dyes [93]. The authors evaluated the photocatalytic potential of similarly sized CDs, but with different compositions and different bandgaps (ranging between 2.63 and 3.63 eV). The three kinds of similarly sized CDs were made using both bottom-up and top-down methodologies, as follows: (1) CD_{OC}-oxidative

cleaving of carbon black; (2) CD_{HP}-hydrothermal pyrolysis of glucose; and (3) CD_{HC}-hydrothermal condensation of pyrene [93]. As intended, and derived from the different synthesis and precursors, the three CDs have considerably different compositions. CD_{OC} had the highest oxygen content (circa 37%), whereas CD_{HC} showed a higher nitrogen content (15%). Moreover, the three CDs had significantly different sp²/sp³ carbon ratios, with the high sp²-carbon content of CD_{HC} suggesting a large amount of highly organized crystalline domains, while CD_{OC} and CD_{HP} seem to have a less organized, more amorphous structure [93]. Regarding the surface functional groups of the CDs, as observed via FTIR, some are common to the three kinds, such as C=C and O-H. Others are specific to each CD: CD_{OC} presents a more oxygenated nature, with C=O and C-O-C groups on its surface; CD_{HP} shows nitrogen-containing bonds, such as C-N and C=N; finally, CD_{HC} showed bands corresponding to C-N and N-H, also suggesting a nitrogen-rich surface [93]. The functional group results show that, as observed by zeta-potential measurements, the CDs are negatively charged in different degrees, namely −23.9 mV for CD_{OC}, −29.4 mV for CD_{HP} and −56.0 mV for CD_{HC}. This negative charge could be important, as it influences the electrostatic interactions between the CDs and the target dye in solution [93].

The absorption spectra of those CDs were analyzed and displayed the typical absorption band at 200–220 nm that corresponds to the excitation of delocalized π electrons in the graphitic sp² into the π^* orbital [99]. Additionally, features at longer wavelengths were also observed and ascribed to n orbitals (originated by the functional groups), which enable n- π^* transitions [100]. The different combinations of functional groups give place to different energy levels and n orbitals, meaning that additional electronic transitions are permitted, which is fundamental for a visible light-driven photocatalyst. A more intense absorption may take place, as seen by the team when they integrated the total absorbance values between 380 and 740 (covering the visible region). CD_{HC} presented the more intense absorption while CD_{HP} presented the least intense absorption. A large difference in terms of absorptivity was observed [93]. Furthermore, the optical bandgaps of the different CDs also varied greatly, with CD_{HP} showing the largest bandgap (3.63 eV-out of the visible range), while CD_{OC} and CD_{HC} presented bandgaps of 2.88 and 2.63 eV, respectively, which are within the visible region [93]. Furthermore, the CDs exhibit excitation-dependent photoluminescence, with the CD_{HP} and CD_{HC} presenting a higher quantum yield (0.10 and 0.44, respectively) than CD_{OC} (0.01), possibly due to the higher degree of functionalization of the latter, is itself a result of the strong oxidizing environment of its synthesis [93].

RhB was used to study the photocatalytic activity of the CDs (Figure 6). Under 6 hours of visible light irradiation, CD_{HC} degraded nearly 55% of the initial pollutant vs. 2% in the absence of the CD. Further experiments revealed that a higher CD_{HC} dosage led to a higher photodegradation yield. The two other CDs, CD_{OC} and CD_{HP}, were less efficient, resulting in a 25% decrease and no decrease whatsoever of the pollutant, respectively. It is worth noting that, under dark conditions, a small amount of RhB (between 4 and 12%) appears to be adsorbed to the CDs, most likely due to the electrostatic interactions between the negatively charged CDs and the cationic dye [93]. The different efficiencies observed for the CDs confirm that factors inherent to each CD, such as chemical composition and crystallization degree, impact the performance of the photocatalysts. The team suggests that the main reason for the differences can be found in each CD capacity of absorbing visible light. CD_{HC} was the most absorbing CD, and so, it was potentially able to originate the largest amount of e⁻h⁺ pairs, an essential step for an efficient photodegradation. On the other hand, CD_{HP} has a relatively large bandgap, preventing the absorption of visible light, and CD_{OC} has an intermediate absorptivity, explaining their respective photocatalytic efficiencies when compared to CD_{HC} [93]. Additionally, the more negative surface of CD_{HC} might favor the adsorption of RhB, and thus facilitate its degradation. The influence of the electrostatic interactions was tested by performing assays with both MB and methyl orange, which are cationic and anionic, respectively. Under visible irradiation, CD_{HC} achieved a 39% MB degradation in 6 hours, whereas only 5% of the methyl orange was degraded [93]. Even though a slight amount of MB was degraded via direct photolysis

(17% when in the absence of CD_{HC}), the negatively charged CD seems to favor the degradation of positively charged dyes. Repulsive interactions difficult the interaction of the CD with methyl orange while favoring the interaction with MB [93]. In summary, the work of Ibarbia et al. highlights the role that parameters such as chemical composition, crystallinity, energy bandgap and light absorptivity have on the photocatalytic efficiency of the resulting CDs. Factors governing the CDs' performance were identified and correlated with the CDs' properties, granting insights valuable for a more rationale design of visible light-driven photocatalytic CDs [93].

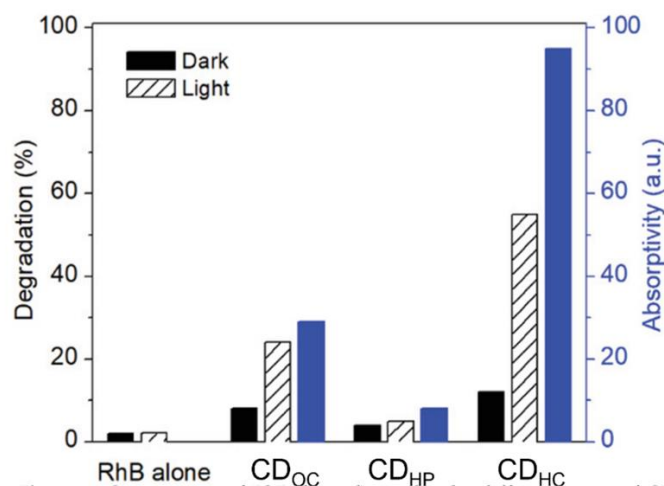


Figure 6. Comparison of RhB degradation by the different types of CDs under 6 hours of visible light irradiation and dark conditions. Reprinted with permission from [93].

The photocatalytic mechanism of CD-driven degradations is mostly similar across the different reports available so far, and comparable to that of semiconductors such as TiO_2 [101]. Generally speaking, the photocatalysts absorb photons of enough energy to overcome their bandgap, which induces the separation of e^-h^+ . These photogenerated charge carriers then migrate to active sites on the photocatalysts, where they react with H_2O and dissolved O_2 . This prompts the generation of ROS, such as $\bullet OH$ and $\bullet O_2^-$. These ROS are an extremely oxidative species with a known power for the degradation of organic pollutants, such as dyes.

A good schematic presentation of the mechanism can be found in the work of Ibarbia et al., who studied that photodegradation of RhB (Figure 7) using three different kinds of CDs and several scavenger species that could react selectively with one type of radical at a time [93]. Additionally, due to the suggestion by some studies that the h^+ might directly degrade dye pollutants [34,86], a possible mechanism based on direct hole transfer from the CDs into the pollutants was also studied via photoluminescence quenching studies in the presence of RhB [93].

The reaction starts when electrons in the CDs' valence band are photoexcited into the conduction band by suitable light. This way, the electron detaches from its corresponding hole and the charge carriers e^- and h^+ are photogenerated and migrate to the CDs' catalytically active sites. Due to the electron donor and acceptor properties of CDs, some of the charge carriers may even be transferred directly to the adsorbed pollutant and initialize the degradation by themselves. However, the charge carriers can also react with H_2O and O_2 adsorbed in the CDs surface to produce ROS. The h^+ interact with adsorbed H_2O to originate $\bullet OH$, whereas the e^- react with O_2 to produce $\bullet O_2^-$. It is also possible that, by its turn, $\bullet O_2^-$ might also react with water and prompt the production of more hydroxyl radicals. In addition, the CDs may also transfer the excited states energy to O_2 to produce highly reactive 1O_2 , which is in line with other studies [102,103]. The team's results suggest that $\bullet OH$ and 1O_2 are the primary radicals in the degradation, whereas $\bullet O_2^-$ may contribute to secondary steps [93].

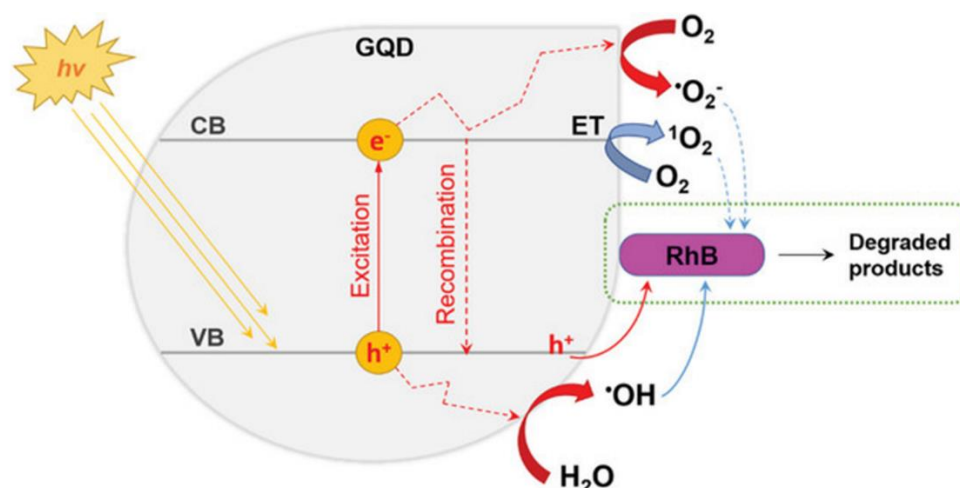


Figure 7. Proposed photodegradation mechanism of a pollutant, RhB, by CDs. Reproduced with authorization from [93].

In summary, there are three potential photodegradation pathways: direct transfer of charge carriers to the adsorbed pollutant; production of highly oxidative ROS via interaction of photogenerated charge carriers with H_2O and dissolved O_2 ; and production of singlet $^1\text{O}_2$ via energy transfer from photoexcited CDs [93]. Ibarbia's suggested mechanism, comprised of both ROS-mediated degradation and direct charge transfer degradation, has been supported by other reports concerning the use of CDs as photocatalytic agents [34,86,104].

2.3. Photocatalytic Photoreduction Reaction and Metal Removal

As previously established, CDs possess several properties that makes them suitable for several applications, among which are the photoreduction reactions and removal of heavy metals. Due to their characteristics, CDs present electron acceptor/donor behaviors, which have been characterized and are known to the scientific community. These studies, focusing on the PL quenching of CDs in the presence of acceptor/donor molecules, promoted a better understanding of the transference of electrons to other species [46,52,105,106].

Cailotto et al. studied these properties using citric acid or citric acid/ethylenediamine-based CDs synthesized via either hydrothermal or pyrolytic treatment [107]. The study permitted the assessment of the photoreduction potential of four CDs, both non-doped and doped, and of an either graphitic or amorphous nature. To this end, the team evaluated the CDs potential to promote the photoreduction of methyl viologen (MV^{2+} to MV^{+}), which is considered as an easy and established way of confirming the photoinduced electron transfer (PET) capacity of CDs via monitoring the absorbance at 605 nm [46,71,108]. The team verified the occurrence of PET between the CDs and methyl viologen, as observed by the quenching of the CDs fluorescence in the presence of increasing concentrations of MV^{2+} . Interestingly, they also observed that the quenching depended heavily on the CDs' nature. Two structural characteristics act independently to favor the CDs' photoredox potential. Purely carbon-based, non-doped CDs are best in photoreducing methyl viologen when their structure is graphitic in nature, as carbonaceous amorphous particles lack photoactive molecules and graphitic defect states capable of promoting electron excitation. By their turn, N-doped CDs' photoredox potential is greatly favored by a more amorphous nature, where nitrogen is incorporated as photoactive molecules responsible for photocatalysis, as a graphitic nature leads to the co-presence of molecular fluorophores and defect states that may quench each other [107]. In another work by the same team [107], the authors once again observed the photoredox potential's dependence on the CDs nature (a graphitic nature favoring non-doped CDs), with the additional finding that, in one of the cases, a reverse structure–activity dependence occurred because of the formation of a large supramolecular graphitic-like assembly [107]. In another study, by Kaushal et al. [56], N-

and N,S-doped CDs were synthesized from citric acid and urea/thiourea via microwave synthesis. By monitoring the photoreduction of methyl viologen, the team found that N-doped CDs present a better photoreduction potential than N,S-doped CDs. As the precursors are equal in everything except the substitution of an O heteroatom by a S heteroatom, the results suggest that single N-doping is a better way of promoting the photoreduction than N,S-co-doping [56].

The visible light/sunlight-driven photocatalytic conversion of CO₂ (via photoreduction) into more valuable materials, such as liquid fuel, could provide a green, sustainable way of decreasing the atmospheric levels of CO₂ [109]. During the CD-mediated photocatalytic conversion of CO₂, upon light absorption, photogenerated e⁻h⁺ charge carriers interact with CO₂ and H₂O through several reactions, causing the production of hydrocarbons (e.g., carbon monoxide, formaldehyde, formic acid, methanol, among others) [110]. Zhao et al. reported the computational and experimental study of the photocatalytic use of 9-hydroxyphenyl-1-one CDs (synthesized via ultrasonic treatment) towards CO₂ photoreduction to CO [111]. The experimental section of the report results in an estimated photocatalytic rate for CO₂ conversion of 5.81 μmol g⁻¹ h⁻¹. The computation section reveals that the formation of COOH•, for which the hydroxyl oxygen atom is the active center, is the rate-limiting step of the conversion [111].

Another practical application of the PET potential displayed by CDs is the photocatalytic reduction of highly toxic hexavalent Cr(VI) to Cr(III), a much less harmful species [53,55,112]. Cr(VI) is a toxic, non-biodegradable, by-product of several industrial processes that is discarded into wastewater where, due to easily mixing with water systems, continuously damages the aquatic system [113–115]. Due to its highly carcinogenic and mutagenic potential, Cr(VI) is considered a prominent threat to human health [116,117]. This is aggravated by the fact that Cr(VI) is conventionally treated via expensive and technically difficult treatments, such as membrane nanofiltration, chemical precipitation and ion exchange [118–120]. However, unlike the hexavalent Cr(VI), Cr(III), its reduced counterpart, is less toxic and is easily removable via adsorption or precipitation as a salt by methods already in existence [121]. Therefore, the conversion of Cr(VI) to Cr(III) via a sustainable method (e.g., sunlight-driven photocatalysis) is highly coveted and needed to remedy the problem. The use of CDs for sensing and biosensing is widely known [27,122,123], in particular, for metal sensing [32,124–126]. Thus, the interaction between CDs and metals, such as chromium, is widely documented. This, in conjugation with the PET properties of CDs, make them suitable candidates for the photoreduction of Cr(VI) and already led to a limited number of publications in this regard [53,55,112].

In 2019, Bhati et al. prepared N,P-doped CDs for the photoreduction of Cr(VI) to Cr(III) [53]. The CDs were made from polyethylene glycol, phosphoric acid and imidazole via microwave-assisted synthesis. The CDs were spherical with an average size of 3.3 nm and presented the expected surface characteristics for a N,P-doped CD, including C-N, C-P, C=N-C, C=N, and O-N/P bindings. The absorption spectra displayed the typical π-π* (210 nm) and n-π* (270 nm) peaks corresponding to C=C and C=N/P, respectively. The CD-catalyzed photoreduction of Cr(VI) under natural sunlight was evaluated. After attaining an adsorption-desorption equilibrium, a nearly complete photoreduction of the initial Cr(VI) concentration was achieved within 110 mins of sunlight irradiation, with the adsorption being responsible for only ~10% of the Cr(VI) decrease [53]. A similar test in the absence of the N,P-doped CDs, in which the changes on the concentration of Cr(VI) (400 ppm) were nearly negligible, confirmed that the CDs were indeed the responsible agent for the photoreduction [53].

Despite the small amount of literature regarding the CD-mediated photoreduction of Cr(VI), another example can be found from the same team in the 2020 work of Saini et al. [55], who fabricated N,S-co-doped CDs from polyethylene glycol, imidazole and thiourea via a microwave-assisted synthesis. The CDs achieved a virtually complete removal of Cr(VI) (initial concentration of 20 ppm) over 90 mins of sunlight irradiation, whereas in dark conditions only a 5% removal of Cr(VI) was observed and in the absence of the CDs, no

removal whatsoever occurred [55]. Increasing the initial concentration of Cr(VI) while maintaining the amount of photocatalyst led to larger removal times (300 mins for 100 ppm), but still ended in a complete removal of Cr(VI). Furthermore, when tested in wastewater samples (from a chemical laboratory and a Cr(VI) spiked industrial sample), Cr(VI) removal was once again efficient, confirming that the photocatalyst is also efficient in complex samples [55]. In a subsequent 2022 report by the same team, Aggarwal et al. fabricated photocatalytic cellulose-based CDs via calcination for Cr(VI) reduction [112]. These CDs, in addition to being photoactive, are based on a readily available natural resource, and so could be an eco-friendly alternative, as they promote a circular economy. Similar to before, the team managed to achieve a virtually complete removal of Cr(VI) (20 ppm) under 120 mins of sunlight irradiation, whereas only 5% was removed in dark conditions and none in the absence of the CDs [112]. Again, larger initial Cr(VI) loading delays the removal, as there is some hindrance preventing the photons from reaching the CDs and there are fewer active sites available for a larger number of Cr(VI) atoms. Finally, the photocatalyst showed reusability for up to four cycles (and the authors suggest that it may be so possibly up to 20 cycles), which is on par with most semiconductor photocatalysts [112]. Despite the similar results in both works, the more recent 2021 report [112] is a step forward in terms of sustainability. Chemical grade reagents are substituted by easily available, environmentally friendlier biomass, and the synthesis, at 90 °C for 30 mins, which is, by CDs standards, much less intensive and shorter than usual (temperatures above 200 °C and times over 2 hours). Considering all this, and the considerable efficiency displayed by the CDs in removing hexavalent Cr(VI) using sunlight irradiation, the overall process can be considered efficient, economical, sustainable, and easy to perform [112].

The team's suggested mechanism for the CD-mediated photoreduction of Cr(VI) (Figure 8) is common across the reviewed articles [53,55,112]. Under visible light irradiation, e^- from the valence band are excited into the conduction band (i), leaving behind a h^+ [53]. The photogenerated h^+ , when recombination is delayed, reacts with water (ii), generating highly reactive H^+ , whereas the e^- initially react with Cr(VI) on the CDs' periphery [53]. The H^+ and e^- cumulatively reduce Cr(VI) to Cr(III) (iii and iv), thus reducing the overall toxicity and enabling precipitation of Cr(III) as a hydroxide salt by adding NaOH [127]. The mechanism was further completed by tests with scavengers for reactive species (hydroxyl radicals, superoxide radicals, e^- and h^+) [55,112]. Regarding the scavenger tests made in the presence of e^- and h^+ scavengers, the Cr(VI) removal via photoreduction is largely inhibited, with removal rates decreasing as much as 73%. On the opposite side, scavengers for other species have a significantly less pronounced effect in Cr(VI) removal, suggesting a more secondary role by these species [55,112].

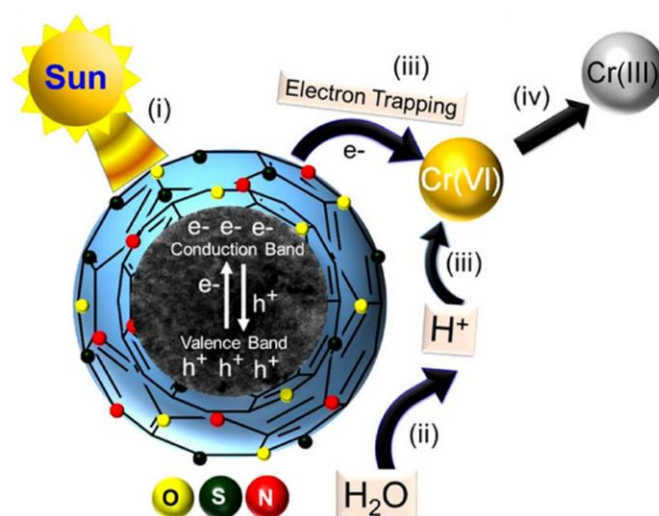


Figure 8. Proposed mechanism for the CD-mediated photoreduction of Cr(VI). Adapted with permission from [55]. Copyright 2020 American Chemical Society.

3. Limitations and Future Challenges

This review focus was to describe studies reporting the use of CDs as sole photocatalysts in diverse applications, namely hydrogen production via water splitting, organic pollutant photodegradation and photoreduction and metal removal. While the benefits of using CDs are notorious, there still several limitations and unanswered questions that limit a wider use of CDs for photocatalysis.

For starters, the CDs were not always properly purified, although the authors denote a clear tendency evolving towards a proper purification of the CDs over the years. A thorough purification for CDs should consist of centrifugation followed by dialysis or chromatography. However, this was not followed in a number of reports. This is quite troublesome, as it is known that bottom-up synthetic routes (e.g., hydrothermal treatment and microwave-assisted synthesis) commonly originate fluorescent molecular impurities/by-products alongside the CDs. These impurities, which are frequently a major part of the products resulting from the CDs' synthesis, can only be efficiently removed by either dialysis or chromatographic purification [18,128]. Moreover, it was observed that these impurities, when not properly removed, can mask, or even modify the properties and reactivity of the CDs [18,128]. Thus, without proper purification, it is uncertain if the photocatalytic effect observed is due to the CDs themselves or due to reactive impurities produced alongside the CDs during the synthesis. Further information in this regard is crucial for a rational and target-oriented synthesis of photocatalytic CDs. Still, in the same topic, despite some good results regarding the use of CDs as photocatalysts, there is still a lack of data regarding how to ensure that the obtained CDs have the desired properties to be an effective photocatalyst. In fact, the available data still do not allow us to determine which synthesis parameters (precursors, route, duration, etc.) are to be chosen (and why) to obtain photocatalytic CDs with good performance, in a rational and well-defined manner.

Furthermore, while CDs are thought to have potential for the photodegradation of organic pollutants, the truth is that most studies in this topic have focused more on organic dyes (such as MB and RhB). This bears the question of how efficient CDs would be to degrade non-dye compounds (such as antibiotics, for example). Furthermore, CDs tend to possess negative charge, which bears the question of how this feature affects the photodegradation of non-cationic compounds. In fact, this could explain why photodegradation studies of CDs tend to focus on cationic dyes (despite some non-cationic dyes still being included).

It should also be considered that the application of photocatalytic CDs in a "real-world" environment requires the successful scale-up of a typically small, laboratory-sized, methodology into a full-scale industrial production procedure. However, CDs synthetic routes typically have a low synthesis yield (commonly below 10%) [129–131]. The reason behind this can be found in the synthetic methodologies most employed by researchers, namely bottom-up strategies such as hydrothermal treatment, which generate large quantities of solid carbon material as a secondary product [129–131]. Recent studies have tried to address this problem by relying on non-conventional procedures to synthesize CDs. This includes adding a eutectic mixture of salts in the carbonization process or subjecting the solid carbon material to a posterior alkaline-peroxide treatment [132,133]. Thus, researchers should also start to focus on increasing the synthesis yield of their CDs, and how processes aimed to do so could affect the properties of these materials. Furthermore, further work is needed to devise strategies capable of recycling a CD photocatalyst in a way that allows its easy recovery and reusability. Current studies regarding recyclability rely on adding more reactants/pollutants to the photocatalytic solution after the previous cycle was finished. While this approach can allow for evaluating the performance of the CDs over different cycles, it does not really allow for recovering the photocatalyst from the reacting mixture.

Last, but not least, a major part of the studies reviewed here used commercially available chemicals, such as the frequently employed citric acid, as the carbon sources for the CDs, with the occasional addition of extra precursors for doping. This is a problem, as recent reports demonstrated that one of the major factors determining the sustainability

and environmental impact of CDs' synthesis is the identity and origin of the carbon source [20,130,131]. Thus, the use of waste material should be preferred as carbon source instead of commercially available chemicals [124,134]. This should favor more circular economy-based approach, in which waste can have a new role instead of just being discarded.

4. Conclusions

This review consisted of a comprehensive study of several areas in which the CDs were already successfully employed as photocatalysts, areas in which they sometimes even excel the more widely used conventional methodologies. Photocatalysis is a process that can be used to make our lives easier. Be it to fulfill our energetic requirements by producing hydrogen or purify our wastewaters from organic pollutants or toxic metals, the option of using an environmentally friendlier and more efficient way of doing so in comparison to conventional methods brings us one step closer to sustainability and carbon neutrality. Due to their properties, CDs are a class of carbon nanomaterials well suited to be used for photocatalysis, as confirmed by several publications that study their use as sole photocatalysts or part of a photocatalytic nanocomposite. Their large absorption region, their PET potential, their low cost and water solubility are all important properties for a photocatalyst. More important is the CDs' capacity of, upon absorption of suitable radiation, to produce photogenerated charge carriers (e^- and h^+). Furthermore, whereas traditional semiconductor photocatalysts require highly energetic UV radiation to work, CDs, due to their excellent optical properties, can work using visible light. The potential of CDs for photocatalysis was reviewed and some limitations were pointed. Further developments in the development of photocatalytic CDs may lead to a cleaner, less wasteful, way of promoting everyday reactions by taking advantage of a renewable energy source, sunlight.

Author Contributions: Conceptualization, R.M.S.S. and L.P.d.S.; writing—original draft preparation, R.M.S.S.; writing—review and editing, L.P.d.S. and J.C.G.E.d.S.; supervision, L.P.d.S. and J.C.G.E.d.S.; funding acquisition, L.P.d.S. and J.C.G.E.d.S. All authors have read and agreed to the published version of the manuscript.

Funding: The Portuguese “Fundação para a Ciência e Tecnologia” (FCT, Lisbon) is acknowledged for funding of project PTDC/QUI-QFI/2870/2020, R&D Units CIQUP (UIDB/00081/2020) and GreenU-Porto (UIDB/05748/2020), and the Associated Laboratory IMS (LA/P/0056/2020). Luís Pinto da Silva acknowledges funding from FCT under the Scientific Employment Stimulus (CEECINST/00069/2021). Ricardo Sendão acknowledges FCT for his Ph.D. grant (2021.06149.BD).

Conflicts of Interest: The authors declare no conflict of interest. The funders had no role in the design of the study; in the collection, analyses, or interpretation of data; in the writing of the manuscript; or in the decision to publish the results.

References

1. Ajayan, P.M. Nanotubes from Carbon. *Chem. Rev.* **1999**, *99*, 1787–1800. [[CrossRef](#)] [[PubMed](#)]
2. Xu, X.; Ray, R.; Gu, Y.; Ploehn, H.J.; Gearheart, L.; Raker, K.; Scrivens, W.A. Electrophoretic analysis and purification of fluorescent single-walled carbon nanotube fragments. *J. Am. Chem. Soc.* **2004**, *126*, 12736–12737. [[CrossRef](#)] [[PubMed](#)]
3. Yang, W.; Ratinac, K.R.; Ringer, S.P.; Thordarson, P.; Gooding, J.J.; Braet, F. Carbon nanomaterials in biosensors: Should you use nanotubes or graphene? *Angew. Chem. Int. Ed. Engl.* **2010**, *49*, 2114–2138. [[CrossRef](#)] [[PubMed](#)]
4. De Jong, K.P.; Geus, J.W. Carbon Nanofibers: Catalytic Synthesis and Applications. *Catal. Rev.* **2007**, *42*, 481–510. [[CrossRef](#)]
5. Liu, Z.; Zhou, X.; Qian, Y. Synthetic methodologies for carbon nanomaterials. *Adv. Mater.* **2010**, *22*, 1963–1966. [[CrossRef](#)] [[PubMed](#)]
6. Rao, C.N.; Sood, A.K.; Subrahmanyam, K.S.; Govindaraj, A. Graphene: The new two-dimensional nanomaterial. *Angew. Chem. Int. Ed. Engl.* **2009**, *48*, 7752–7777. [[CrossRef](#)]
7. Kroto, H.W.; Heath, J.R.; O'Brien, S.C.; Curl, R.F.; Smalley, R.E. C_{60} : Buckminsterfullerene. *Nature* **1985**, *318*, 162–163. [[CrossRef](#)]
8. Sun, Y.P.; Zhou, B.; Lin, Y.; Wang, W.; Fernando, K.A.; Pathak, P.; Mezziani, M.J.; Harruff, B.A.; Wang, X.; Wang, H.; et al. Quantum-sized carbon dots for bright and colorful photoluminescence. *J. Am. Chem. Soc.* **2006**, *128*, 7756–7757. [[CrossRef](#)]
9. da Silva, J.C.G.E.; Gonçalves, H.M.R. Analytical and bioanalytical applications of carbon dots. *TrAC Trends. Anal. Chem.* **2011**, *30*, 1327–1336. [[CrossRef](#)]
10. Hola, K.; Zhang, Y.; Wang, Y.; Giannelis, E.P.; Zboril, R.; Rogach, A.L. Carbon dots—Emerging light emitters for bioimaging, cancer therapy and optoelectronics. *Nano Today* **2014**, *9*, 590–603. [[CrossRef](#)]

11. Baker, S.N.; Baker, G.A. Luminescent carbon nanodots: Emergent nanolights. *Angew. Chem. Int. Ed. Engl.* **2010**, *49*, 6726–6744. [[CrossRef](#)] [[PubMed](#)]
12. Demchenko, A.P.; Dekaliuk, M.O. Novel fluorescent carbonic nanomaterials for sensing and imaging. *Methods Appl. Fluoresc.* **2013**, *1*, 042001. [[CrossRef](#)] [[PubMed](#)]
13. Crista, D.M.A.; Esteves da Silva, J.C.G.; Pinto da Silva, L. Evaluation of Different Bottom-up Routes for the Fabrication of Carbon Dots. *Nanomaterials* **2020**, *10*, 1316. [[CrossRef](#)]
14. Tan, M.; Zhang, L.; Tang, R.; Song, X.; Li, Y.; Wu, H.; Wang, Y.; Lv, G.; Liu, W.; Ma, X. Enhanced photoluminescence and characterization of multicolor carbon dots using plant soot as a carbon source. *Talanta* **2013**, *115*, 950–956. [[CrossRef](#)]
15. Wang, J.; Sahu, S.; Sonkar, S.K.; Tackett II, K.N.; Sun, K.W.; Liu, Y.; Maimaiti, H.; Anilkumar, P.; Sun, Y.-P. Versatility with carbon dots—From overcooked BBQ to brightly fluorescent agents and photocatalysts. *RSC Adv.* **2013**, *3*, 15604–15607. [[CrossRef](#)]
16. Lu, J.; Yang, J.X.; Wang, J.; Lim, A.; Wang, S.; Loh, K.P. One-pot synthesis of fluorescent carbon nanoribbons, nanoparticles, and graphene by the exfoliation of graphite in ionic liquids. *ACS Nano* **2009**, *3*, 2367–2375. [[CrossRef](#)]
17. Park, S.Y.; Lee, H.U.; Park, E.S.; Lee, S.C.; Lee, J.W.; Jeong, S.W.; Kim, C.H.; Lee, Y.C.; Huh, Y.S.; Lee, J. Photoluminescent green carbon nanodots from food-waste-derived sources: Large-scale synthesis, properties, and biomedical applications. *ACS Appl. Mater. Interfaces* **2014**, *6*, 3365–3370. [[CrossRef](#)]
18. Sendao, R.M.S.; Crista, D.M.A.; Afonso, A.C.P.; Martinez de Yuso, M.D.V.; Algarra, M.; Esteves da Silva, J.C.G.; Pinto da Silva, L. Insight into the hybrid luminescence showed by carbon dots and molecular fluorophores in solution. *Phys. Chem. Chem. Phys.* **2019**, *21*, 20919–20926. [[CrossRef](#)]
19. Ma, C.B.; Zhu, Z.T.; Wang, H.X.; Huang, X.; Zhang, X.; Qi, X.; Zhang, H.L.; Zhu, Y.; Deng, X.; Peng, Y.; et al. A general solid-state synthesis of chemically-doped fluorescent graphene quantum dots for bioimaging and optoelectronic applications. *Nanoscale* **2015**, *7*, 10162–10169. [[CrossRef](#)]
20. Sendão, R.; Yuso, M.d.V.M.d.; Algarra, M.; Esteves da Silva, J.C.G.; Pinto da Silva, L. Comparative life cycle assessment of bottom-up synthesis routes for carbon dots derived from citric acid and urea. *J. Clean. Prod.* **2020**, *254*, 120080. [[CrossRef](#)]
21. Liu, R.; Wu, D.; Liu, S.; Koynov, K.; Knoll, W.; Li, Q. An aqueous route to multicolor photoluminescent carbon dots using silica spheres as carriers. *Angew. Chem. Int. Ed. Engl.* **2009**, *48*, 4598–4601. [[CrossRef](#)] [[PubMed](#)]
22. Jiang, H.; Chen, F.; Lagally, M.G.; Denes, F.S. New strategy for synthesis and functionalization of carbon nanoparticles. *Langmuir* **2010**, *26*, 1991–1995. [[CrossRef](#)] [[PubMed](#)]
23. Long, C.; Jiang, Z.; Shangguan, J.; Qing, T.; Zhang, P.; Feng, B. Applications of carbon dots in environmental pollution control: A review. *Chem. Eng. J.* **2021**, *406*, 126848. [[CrossRef](#)]
24. Wang, R.; Lu, K.-Q.; Tang, Z.-R.; Xu, Y.-J. Recent progress in carbon quantum dots: Synthesis, properties and applications in photocatalysis. *J. Mater. Chem. A* **2017**, *5*, 3717–3734. [[CrossRef](#)]
25. Peng, Z.; Han, X.; Li, S.; Al-Youbi, A.O.; Bashammakh, A.S.; El-Shahawi, M.S.; Leblanc, R.M. Carbon dots: Biomacromolecule interaction, bioimaging and nanomedicine. *Coord. Chem. Rev.* **2017**, *343*, 256–277. [[CrossRef](#)]
26. Lim, S.Y.; Shen, W.; Gao, Z. Carbon quantum dots and their applications. *Chem. Soc. Rev.* **2015**, *44*, 362–381. [[CrossRef](#)]
27. Vale, N.; Silva, S.; Duarte, D.; Crista, D.M.A.; Pinto da Silva, L.; Esteves da Silva, J.C.G. Normal breast epithelial MCF-10A cells to evaluate the safety of carbon dots. *RSC Med. Chem.* **2021**, *12*, 245–253. [[CrossRef](#)]
28. Wang, K.; Gao, Z.; Gao, G.; Wo, Y.; Wang, Y.; Shen, G.; Cui, D. Systematic safety evaluation on photoluminescent carbon dots. *Nanoscale Res. Lett.* **2013**, *8*, 122. [[CrossRef](#)]
29. Deng, Y.; Chen, M.; Chen, G.; Zou, W.; Zhao, Y.; Zhang, H.; Zhao, Q. Visible-Ultraviolet Upconversion Carbon Quantum Dots for Enhancement of the Photocatalytic Activity of Titanium Dioxide. *ACS Omega* **2021**, *6*, 4247–4254. [[CrossRef](#)]
30. Dager, A.; Uchida, T.; Maekawa, T.; Tachibana, M. Synthesis and characterization of Mono-disperse Carbon Quantum Dots from Fennel Seeds: Photoluminescence analysis using Machine Learning. *Sci. Rep.* **2019**, *9*, 14004. [[CrossRef](#)]
31. Ladomenou, K.; Landrou, G.; Charalambidis, G.; Nikoloudakis, E.; Coutsolelos, A.G. Carbon dots for photocatalytic H₂ production in aqueous media with molecular Co catalysts. *Sustain. Energy Fuels* **2021**, *5*, 449–458. [[CrossRef](#)]
32. Yang, P.; Zhao, J.; Wang, J.; Cao, B.; Li, L.; Zhu, Z. Light-induced synthesis of photoluminescent carbon nanoparticles for Fe³⁺ sensing and photocatalytic hydrogen evolution. *J. Mater. Chem. A* **2015**, *3*, 136–138. [[CrossRef](#)]
33. Bhunia, S.; Ghorai, N.; Burai, S.; Purkayastha, P.; Ghosh, H.N.; Mondal, S. Unraveling the Carrier Dynamics and Photocatalytic Pathway in Carbon Dots and Pollutants of Wastewater System. *J. Phys. Chem. C* **2021**, *125*, 27252–27259. [[CrossRef](#)]
34. Zhou, Y.; Zahran, E.M.; Quiroga, B.A.; Perez, J.; Mintz, K.J.; Peng, Z.; Liyanage, P.Y.; Pandey, R.R.; Chusuei, C.C.; Leblanc, R.M. Size-Dependent Photocatalytic Activity of Carbon Dots with Surface-State Determined Photoluminescence. *Appl. Catal. B* **2019**, *248*, 157–166. [[CrossRef](#)]
35. Zhang, F.; Wang, X.; Liu, H.; Liu, C.; Wan, Y.; Long, Y.; Cai, Z. Recent Advances and Applications of Semiconductor Photocatalytic Technology. *Appl. Sci.* **2019**, *9*, 2489. [[CrossRef](#)]
36. Zhang, Z.; Zheng, T.; Li, X.; Xu, J.; Zeng, H. Progress of Carbon Quantum Dots in Photocatalysis Applications. *Part. Part. Syst. Charact.* **2016**, *33*, 457–472. [[CrossRef](#)]
37. Linsebigler, A.L.; Lu, G.; Yates, J.T. Photocatalysis on TiO₂ Surfaces: Principles, Mechanisms, and Selected Results. *Chem. Rev.* **2002**, *95*, 735–758. [[CrossRef](#)]
38. Yang, K.D.; Ha, Y.; Sim, U.; An, J.; Lee, C.W.; Jin, K.; Kim, Y.; Park, J.; Hong, J.S.; Lee, J.H.; et al. Graphene Quantum Sheet Catalyzed Silicon Photocathode for Selective CO₂ Conversion to CO. *Adv. Funct. Mater.* **2016**, *26*, 233–242. [[CrossRef](#)]

39. Gao, G.; Jiao, Y.; Ma, F.; Jiao, Y.; Waclawik, E.; Du, A. Carbon nanodot decorated graphitic carbon nitride: New insights into the enhanced photocatalytic water splitting from ab initio studies. *Phys. Chem. Chem. Phys.* **2015**, *17*, 31140–31144. [[CrossRef](#)]
40. Yeh, T.F.; Teng, C.Y.; Chen, S.J.; Teng, H. Nitrogen-doped graphene oxide quantum dots as photocatalysts for overall water-splitting under visible light illumination. *Adv. Mater.* **2014**, *26*, 3297–3303. [[CrossRef](#)]
41. Qu, D.; Sun, Z.; Zheng, M.; Li, J.; Zhang, Y.; Zhang, G.; Zhao, H.; Liu, X.; Xie, Z. Three Colors Emission from S,N Co-doped Graphene Quantum Dots for Visible Light H₂ Production and Bioimaging. *Adv. Opt. Mater.* **2015**, *3*, 360–367. [[CrossRef](#)]
42. Yu, H.; Shi, R.; Zhao, Y.; Waterhouse, G.I.; Wu, L.Z.; Tung, C.H.; Zhang, T. Smart Utilization of Carbon Dots in Semiconductor Photocatalysis. *Adv. Mater.* **2016**, *28*, 9454–9477. [[CrossRef](#)] [[PubMed](#)]
43. Chai, N.-N.; Wang, H.-X.; Hu, C.-X.; Wang, Q.; Zhang, H.-L. Well-controlled layer-by-layer assembly of carbon dot/CdS heterojunctions for efficient visible-light-driven photocatalysis. *J. Mater. Chem. A* **2015**, *3*, 16613–16620. [[CrossRef](#)]
44. Di, J.; Xia, J.; Ji, M.; Wang, B.; Yin, S.; Zhang, Q.; Chen, Z.; Li, H. Carbon Quantum Dots Modified BiOCl Ultrathin Nanosheets with Enhanced Molecular Oxygen Activation Ability for Broad Spectrum Photocatalytic Properties and Mechanism Insight. *ACS Appl. Mater. Interfaces* **2015**, *7*, 20111–20123. [[CrossRef](#)] [[PubMed](#)]
45. Zhang, H.; Huang, H.; Ming, H.; Li, H.; Zhang, L.; Liu, Y.; Kang, Z. Carbon quantum dots/Ag₃PO₄ complex photocatalysts with enhanced photocatalytic activity and stability under visible light. *J. Mater. Chem.* **2012**, *22*, 10501–10506. [[CrossRef](#)]
46. Martindale, B.C.; Hutton, G.A.; Caputo, C.A.; Reischer, E. Solar hydrogen production using carbon quantum dots and a molecular nickel catalyst. *J. Am. Chem. Soc.* **2015**, *137*, 6018–6025. [[CrossRef](#)]
47. Qu, D.; Zheng, M.; Du, P.; Zhou, Y.; Zhang, L.; Li, D.; Tan, H.; Zhao, Z.; Xie, Z.; Sun, Z. Highly luminescent S, N co-doped graphene quantum dots with broad visible absorption bands for visible light photocatalysts. *Nanoscale* **2013**, *5*, 12272–12277. [[CrossRef](#)]
48. Yu, H.; Zhao, Y.; Zhou, C.; Shang, L.; Peng, Y.; Cao, Y.; Wu, L.-Z.; Tung, C.-H.; Zhang, T. Carbon quantum dots/TiO₂ composites for efficient photocatalytic hydrogen evolution. *J. Mater. Chem. A* **2014**, *2*, 3344–3351. [[CrossRef](#)]
49. Yu, X.; Liu, J.; Yu, Y.; Zuo, S.; Li, B. Preparation and visible light photocatalytic activity of carbon quantum dots/TiO₂ nanosheet composites. *Carbon* **2014**, *68*, 718–724. [[CrossRef](#)]
50. Pan, J.; Sheng, Y.; Zhang, J.; Wei, J.; Huang, P.; Zhang, X.; Feng, B. Preparation of carbon quantum dots/TiO₂ nanotubes composites and their visible light catalytic applications. *J. Mater. Chem. A* **2014**, *2*, 18082–18086. [[CrossRef](#)]
51. Guo, Y.; Yao, P.; Zhu, D.; Gu, C. A novel method for the development of a carbon quantum dot/carbon nitride hybrid photocatalyst that responds to infrared light irradiation. *J. Mater. Chem. A* **2015**, *3*, 13189–13192. [[CrossRef](#)]
52. Campalani, C.; Cattaruzza, E.; Zorzi, S.; Vomiero, A.; You, S.; Matthews, L.; Capron, M.; Mondelli, C.; Selva, M.; Perosa, A. Biobased Carbon Dots: From Fish Scales to Photocatalysis. *Nanomaterials* **2021**, *11*, 524. [[CrossRef](#)] [[PubMed](#)]
53. Bhati, A.; Anand, S.R.; Saini, D.; Gunture; Sonkar, S.K. Sunlight-induced photoreduction of Cr(VI) to Cr(III) in wastewater by nitrogen-phosphorus-doped carbon dots. *NPJ Clean Water* **2019**, *2*, 12. [[CrossRef](#)]
54. Zhu, Z.; Li, X.; Luo, M.; Chen, M.; Chen, W.; Yang, P.; Zhou, X. Synthesis of carbon dots with high photocatalytic reactivity by tailoring heteroatom doping. *J. Colloid Interface Sci.* **2022**, *605*, 330–341. [[CrossRef](#)]
55. Saini, D.; Kaushik, J.; Garg, A.K.; Dalal, C.; Sonkar, S.K. N, S-codoped Carbon Dots for Nontoxic Cell Imaging and As a Sunlight-Active Photocatalytic Material for the Removal of Chromium. *ACS Appl. Bio. Mater.* **2020**, *3*, 3656–3663. [[CrossRef](#)]
56. Kaushal, N.; Sharma, A.L.; Saha, A. Visible LED-based photo-redox properties of sulfur and nitrogen-doped carbon dots designed by solid-state synthesis. *Mater. Adv.* **2022**, *3*, 355–361. [[CrossRef](#)]
57. Zhou, Y.; ElMetwally, A.E.; Chen, J.; Shi, W.; Cilingir, E.K.; Walters, B.; Mintz, K.J.; Martin, C.; Ferreira, B.; Zhang, W.; et al. Gel-like carbon dots: A high-performance future photocatalyst. *J. Colloid Interface Sci.* **2021**, *599*, 519–532. [[CrossRef](#)]
58. Genc, M.T.; Yanalak, G.; Aksoy, I.; Aslan, E.; Patir, I.H. Green Carbon Dots (GCDs) for Photocatalytic Hydrogen Evolution and Antibacterial Applications. *Chem. Sel.* **2021**, *6*, 7317–7322. [[CrossRef](#)]
59. Jana, B.; Reva, Y.; Scharl, T.; Strauss, V.; Cadranel, A.; Guldi, D.M. Carbon Nanodots for All-in-One Photocatalytic Hydrogen Generation. *J. Am. Chem. Soc.* **2021**, *143*, 20122–20132. [[CrossRef](#)]
60. Xu, X.; Bao, Z.; Zhou, G.; Zeng, H.; Hu, J. Enriching Photoelectrons via Three Transition Channels in Amino-Conjugated Carbon Quantum Dots to Boost Photocatalytic Hydrogen Generation. *ACS Appl. Mater. Interfaces* **2016**, *8*, 14118–14124. [[CrossRef](#)]
61. Saini, D.; Aggarwal, R.; Sonker, A.K.; Sonkar, S.K. Photodegradation of Azo Dyes in Sunlight Promoted by Nitrogen–Sulfur–Phosphorus Codoped Carbon Dots. *ACS Appl. Nano Mater.* **2021**, *4*, 9303–9312. [[CrossRef](#)]
62. Fujishima, A.; Honda, K. Electrochemical photolysis of water at a semiconductor electrode. *Nature* **1972**, *238*, 37–38. [[CrossRef](#)]
63. Li, X.; Yu, J.; Low, J.; Fang, Y.; Xiao, J.; Chen, X. Engineering heterogeneous semiconductors for solar water splitting. *J. Mater. Chem. A* **2015**, *3*, 2485–2534. [[CrossRef](#)]
64. Reddy, C.V.; Reddy, K.R.; Harish, V.V.N.; Shim, J.; Shankar, M.V.; Shetti, N.P.; Aminabhavi, T.M. Metal-organic frameworks (MOFs)-based efficient heterogeneous photocatalysts: Synthesis, properties and its applications in photocatalytic hydrogen generation, CO₂ reduction and photodegradation of organic dyes. *Int. J. Hydrogen Energy* **2020**, *45*, 7656–7679. [[CrossRef](#)]
65. Chen, X.; Shen, S.; Guo, L.; Mao, S.S. Semiconductor-based photocatalytic hydrogen generation. *Chem. Rev.* **2010**, *110*, 6503–6570. [[CrossRef](#)] [[PubMed](#)]
66. Yang, P.; Zhao, J.; Wang, J.; Cui, H.; Li, L.; Zhu, Z. Pure carbon nanodots for excellent photocatalytic hydrogen generation. *RSC Adv.* **2015**, *5*, 21332–21335. [[CrossRef](#)]

67. Cao, L.; Sahu, S.; Anilkumar, P.; Bunker, C.E.; Xu, J.; Fernando, K.A.; Wang, P.; Gulians, E.A.; Tackett, K.N., 2nd; Sun, Y.P. Carbon nanoparticles as visible-light photocatalysts for efficient CO₂ conversion and beyond. *J. Am. Chem. Soc.* **2011**, *133*, 4754–4757. [[CrossRef](#)] [[PubMed](#)]
68. Bhattacharyya, S.; Ehrat, F.; Urban, P.; Teves, R.; Wyrwich, R.; Doblinger, M.; Feldmann, J.; Urban, A.S.; Stolarczyk, J.K. Effect of nitrogen atom positioning on the trade-off between emissive and photocatalytic properties of carbon dots. *Nat. Commun.* **2017**, *8*, 1401. [[CrossRef](#)] [[PubMed](#)]
69. Carlsen, L.; Bruggemann, R.; Sailaukhanuly, Y. Application of selected partial order tools to analyze fate and toxicity indicators of environmentally hazardous chemicals. *Ecol. Indic.* **2013**, *29*, 191–202. [[CrossRef](#)]
70. Richardson, S.D. Environmental mass spectrometry: Emerging contaminants and current issues. *Anal. Chem.* **2012**, *84*, 747–778. [[CrossRef](#)]
71. Rigodanza, F.; Dorđević, L.; Arcudi, F.; Prato, M. Customizing the Electrochemical Properties of Carbon Nanodots by Using Quinones in Bottom-Up Synthesis. *Angew. Chem.* **2018**, *130*, 5156–5161. [[CrossRef](#)]
72. Liu, Q.; Zhou, Y.; Lu, J.; Zhou, Y. Novel cyclodextrin-based adsorbents for removing pollutants from wastewater: A critical review. *Chemosphere* **2020**, *241*, 125043. [[CrossRef](#)] [[PubMed](#)]
73. Mekonnen, M.M.; Hoekstra, A.Y. Four billion people facing severe water scarcity. *Sci. Adv.* **2016**, *2*, e1500323. [[CrossRef](#)] [[PubMed](#)]
74. Tollefson, J. How green is my future? *Nature* **2011**, *473*, 134–135. [[CrossRef](#)] [[PubMed](#)]
75. Sendao, R.M.S.; Esteves da Silva, J.C.G.; Pinto da Silva, L. Photocatalytic removal of pharmaceutical water pollutants by TiO₂–Carbon dots nanocomposites: A review. *Chemosphere* **2022**, *301*, 134731. [[CrossRef](#)]
76. Sharma, S.; Dutta, V.; Singh, P.; Raizada, P.; Rahmani-Sani, A.; Hosseini-Bandegharai, A.; Thakur, V.K. Carbon quantum dot supported semiconductor photocatalysts for efficient degradation of organic pollutants in water: A review. *J. Clean. Prod.* **2019**, *228*, 755–769. [[CrossRef](#)]
77. Umrao, S.; Sharma, P.; Bansal, A.; Sinha, R.; Singh, R.K.; Srivastava, A. Multi-layered graphene quantum dots derived photodegradation mechanism of methylene blue. *RSC Adv.* **2015**, *5*, 51790–51798. [[CrossRef](#)]
78. Zhu, Z.; Yang, P.; Li, X.; Luo, M.; Zhang, W.; Chen, M.; Zhou, X. Green preparation of palm powder-derived carbon dots co-doped with sulfur/chlorine and their application in visible-light photocatalysis. *Spectrochim. Acta A Mol. Biomol. Spectrosc.* **2020**, *227*, 117659. [[CrossRef](#)]
79. Hu, Y.; Guan, R.; Zhang, C.; Zhang, K.; Liu, W.; Shao, X.; Xue, Q.; Yue, Q. Fluorescence and photocatalytic activity of metal-free nitrogen-doped carbon quantum dots with varying nitrogen contents. *Appl. Surf. Sci.* **2020**, *531*, 147344. [[CrossRef](#)]
80. Sharma, S.; Ibhaddon, A.O.; Francesconi, M.G.; Mehta, S.K.; Elumalai, S.; Kansal, S.K.; Umar, A.; Baskoutas, S. Bi₂WO₆/C-Dots/TiO₂: A Novel Z-Scheme Photocatalyst for the Degradation of Fluoroquinolone Levofloxacin from Aqueous Medium. *Nanomaterials* **2020**, *10*, 910. [[CrossRef](#)]
81. Sharma, S.; Umar, A.; Mehta, S.K.; Ibhaddon, A.O.; Kansal, S.K. Solar light driven photocatalytic degradation of levofloxacin using TiO₂/carbon-dot nanocomposites. *New J. Chem.* **2018**, *42*, 7445–7456. [[CrossRef](#)]
82. Wongso, V.; Chung, H.K.; Sambudi, N.S.; Sufian, S.; Abdullah, B.; Wirzal, M.D.H.; Ang, W.L. Silica–carbon quantum dots decorated titanium dioxide as sunlight-driven photocatalyst to diminish acetaminophen from aquatic environment. *J. Photochem. Photobiol. A Chem.* **2020**, *394*, 112436. [[CrossRef](#)]
83. Koe, W.S.; Chong, W.C.; Pang, Y.L.; Koo, C.H.; Ebrahim, M.; Mohammad, A.W. Novel nitrogen and sulphur co-doped carbon quantum dots/titanium oxide photocatalytic membrane for in-situ degradation and removal of pharmaceutical compound. *J. Water Process Eng.* **2020**, *33*, 101068. [[CrossRef](#)]
84. Aggarwal, R.; Saini, D.; Singh, B.; Kaushik, J.; Garg, A.K.; Sonkar, S.K. Bitter apple peel derived photoactive carbon dots for the sunlight induced photocatalytic degradation of crystal violet dye. *Sol. Energy* **2020**, *197*, 326–331. [[CrossRef](#)]
85. Zhang, S.; Fan, X.; Guan, R.; Hu, Y.; Jiang, S.; Shao, X.; Wang, S.; Yue, Q. Carbon dots as metal-free photocatalyst for dye degradation with high efficiency within nine minutes in dark. *Opt. Mater.* **2022**, *123*, 111914. [[CrossRef](#)]
86. Huang, B.; He, J.; Bian, S.; Zhou, C.; Li, Z.; Xi, F.; Liu, J.; Dong, X. S-doped graphene quantum dots as nanophotocatalyst for visible light degradation. *Chin. Chem. Lett.* **2018**, *29*, 1698–1701. [[CrossRef](#)]
87. Umrao, S.; Abraham, S.; Theil, F.; Pandey, S.; Ciobota, V.; Shukla, P.K.; Rupp, C.J.; Chakraborty, S.; Ahuja, R.; Popp, J.; et al. A possible mechanism for the emergence of an additional band gap due to a Ti–O–C bond in the TiO₂–graphene hybrid system for enhanced photodegradation of methylene blue under visible light. *RSC Adv.* **2014**, *4*, 59890–59901. [[CrossRef](#)]
88. Yashwanth, H.J.; Rondiya, S.R.; Dzade, N.Y.; Dhole, S.D.; Phase, D.M.; Hareesh, K. Enhanced photocatalytic activity of N, P, co-doped carbon quantum dots: An insight from experimental and computational approach. *Vacuum* **2020**, *180*, 109589. [[CrossRef](#)]
89. Peng, Z.; Zhou, Y.; Ji, C.; Pardo, J.; Mintz, K.J.; Pandey, R.R.; Chusuei, C.C.; Graham, R.M.; Yan, G.; Leblanc, R.M. Facile Synthesis of “Boron-Doped” Carbon Dots and Their Application in Visible-Light-Driven Photocatalytic Degradation of Organic Dyes. *Nanomaterials* **2020**, *10*, 1560. [[CrossRef](#)]
90. Bramhaiah, K.; Bhuyan, R.; Mandal, S.; Kar, S.; Prabhu, R.; John, N.S.; Gramlich, M.; Urban, A.S.; Bhattacharyya, S. Molecular, Aromatic, and Amorphous Domains of N-Carbon Dots: Leading toward the Competitive Photoluminescence and Photocatalytic Properties. *J. Phys. Chem. C* **2021**, *125*, 4299–4309. [[CrossRef](#)]
91. Das, G.S.; Shim, J.P.; Bhatnagar, A.; Tripathi, K.M.; Kim, T. Biomass-derived Carbon Quantum Dots for Visible-Light-Induced Photocatalysis and Label-Free Detection of Fe(III) and Ascorbic acid. *Sci. Rep.* **2019**, *9*, 15084. [[CrossRef](#)]

92. Aghamali, A.; Khosravi, M.; Hamishehkar, H.; Modirshahla, N.; Behnajady, M.A. Synthesis and characterization of high efficient photoluminescent sunlight driven photocatalyst of N-Carbon Quantum Dots. *J. Lumin.* **2018**, *201*, 265–274. [[CrossRef](#)]
93. Ibarbia, A.; Grande, H.J.; Ruiz, V. On the Factors behind the Photocatalytic Activity of Graphene Quantum Dots for Organic Dye Degradation. *Part. Part. Syst. Charact.* **2020**, *37*, 2000061. [[CrossRef](#)]
94. Ma, Z.; Ming, H.; Huang, H.; Liu, Y.; Kang, Z. One-step ultrasonic synthesis of fluorescent N-doped carbon dots from glucose and their visible-light sensitive photocatalytic ability. *New J. Chem.* **2012**, *36*, 861–864. [[CrossRef](#)]
95. Wang, C.; Xu, J.; Zhang, R.; Zhao, W. Facile and low-energy-consumption synthesis of dual-functional carbon dots from *Cornus walteri* leaves for detection of p-nitrophenol and photocatalytic degradation of dyes. *Colloids Surf. A Physicochem. Eng. Asp.* **2022**, *640*, 128351. [[CrossRef](#)]
96. Smrithi, S.P.; Kottam, N.; Vergis, B.R. Heteroatom Modified Hybrid Carbon Quantum Dots Derived from Cucurbita pepo for the Visible Light Driven Photocatalytic Dye Degradation. *Top. Catal.* **2022**. [[CrossRef](#)]
97. Hu, S.; Tian, R.; Wu, L.; Zhao, Q.; Yang, J.; Liu, J.; Cao, S. Chemical regulation of carbon quantum dots from synthesis to photocatalytic activity. *Chem. Asian J.* **2013**, *8*, 1035–1041. [[CrossRef](#)]
98. Sabet, M.; Mahdavi, K. Green synthesis of high photoluminescence nitrogen-doped carbon quantum dots from grass via a simple hydrothermal method for removing organic and inorganic water pollutants. *Appl. Surf. Sci.* **2019**, *463*, 283–291. [[CrossRef](#)]
99. Bacon, M.; Bradley, S.J.; Nann, T. Graphene Quantum Dots. *Part. Part. Syst. Charact.* **2014**, *31*, 415–428. [[CrossRef](#)]
100. Yan, Y.; Chen, J.; Li, N.; Tian, J.; Li, K.; Jiang, J.; Liu, J.; Tian, Q.; Chen, P. Systematic Bandgap Engineering of Graphene Quantum Dots and Applications for Photocatalytic Water Splitting and CO₂ Reduction. *ACS Nano* **2018**, *12*, 3523–3532. [[CrossRef](#)]
101. Lee, S.-Y.; Park, S.-J. TiO₂ photocatalyst for water treatment applications. *J. Ind. Eng. Chem.* **2013**, *19*, 1761–1769. [[CrossRef](#)]
102. Zhang, J.; Wu, S.; Lu, X.; Wu, P.; Liu, J. Lanthanide-Boosted Singlet Oxygen from Diverse Photosensitizers along with Potent Photocatalytic Oxidation. *ACS Nano* **2019**, *13*, 14152–14161. [[CrossRef](#)] [[PubMed](#)]
103. Ge, J.; Lan, M.; Zhou, B.; Liu, W.; Guo, L.; Wang, H.; Jia, Q.; Niu, G.; Huang, X.; Zhou, H.; et al. A graphene quantum dot photodynamic therapy agent with high singlet oxygen generation. *Nat. Commun.* **2014**, *5*, 4596. [[CrossRef](#)]
104. Fan, J.; Li, D.; Wang, X. Effect of modified graphene quantum dots on photocatalytic degradation property. *Diamond Relat. Mater.* **2016**, *69*, 81–85. [[CrossRef](#)]
105. Hutton, G.A.; Reuillard, B.; Martindale, B.C.; Caputo, C.A.; Lockwood, C.W.; Butt, J.N.; Reisner, E. Carbon Dots as Versatile Photosensitizers for Solar-Driven Catalysis with Redox Enzymes. *J. Am. Chem. Soc.* **2016**, *138*, 16722–16730. [[CrossRef](#)]
106. Mondal, S.; Das, T.; Maity, A.; Seth, S.K.; Purkayastha, P. Synergic Influence of Reverse Micelle Confinement on the Enhancement in Photoinduced Electron Transfer to and from Carbon Nanoparticles. *J. Phys. Chem. C* **2015**, *119*, 13887–13892. [[CrossRef](#)]
107. Amadio, E.; Cailotto, S.; Campalani, C.; Branzi, L.; Raviola, C.; Ravelli, D.; Cattaruzza, E.; Trave, E.; Benedetti, A.; Selva, M.; et al. Precursor-Dependent Photocatalytic Activity of Carbon Dots. *Molecules* **2019**, *25*, 101. [[CrossRef](#)]
108. Martindale, B.C.M.; Hutton, G.A.M.; Caputo, C.A.; Prantl, S.; Godin, R.; Durrant, J.R.; Reisner, E. Enhancing Light Absorption and Charge Transfer Efficiency in Carbon Dots through Graphitization and Core Nitrogen Doping. *Angew. Chem. Int. Ed. Engl.* **2017**, *56*, 6459–6463. [[CrossRef](#)]
109. Fernando, K.A.; Sahu, S.; Liu, Y.; Lewis, W.K.; Gulians, E.A.; Jafariyan, A.; Wang, P.; Bunker, C.E.; Sun, Y.P. Carbon quantum dots and applications in photocatalytic energy conversion. *ACS Appl. Mater. Interfaces* **2015**, *7*, 8363–8376. [[CrossRef](#)]
110. Sahara, G.; Ishitani, O. Efficient Photocatalysts for CO₂ Reduction. *Inorg. Chem.* **2015**, *54*, 5096–5104. [[CrossRef](#)]
111. Zhao, Z.; Zhang, H.; Song, X.; Shi, Y.; Si, D.; Li, H.; Hao, C. Insight into the CO₂ photoreduction mechanism over 9-hydroxyphenal-1-one (HPHN) carbon quantum dots. *J. Energy Chem.* **2021**, *52*, 269–276. [[CrossRef](#)]
112. Aggarwal, R.; Saini, D.; Sonkar, S.K.; Sonker, A.K.; Westman, G. Sunlight promoted removal of toxic hexavalent chromium by cellulose derived photoactive carbon dots. *Chemosphere* **2022**, *287*, 132287. [[CrossRef](#)] [[PubMed](#)]
113. Omole, M.A.; K’Owino, I.O.; Sadik, O.A. Palladium nanoparticles for catalytic reduction of Cr(VI) using formic acid. *Appl. Catal. B Environ.* **2007**, *76*, 158–167. [[CrossRef](#)]
114. Yang, Y.; Wang, G.; Deng, Q.; Ng, D.H.; Zhao, H. Microwave-assisted fabrication of nanoparticulate TiO₂ microspheres for synergistic photocatalytic removal of Cr(VI) and methyl orange. *ACS Appl. Mater. Interfaces* **2014**, *6*, 3008–3015. [[CrossRef](#)]
115. Abdullah, H.; Kuo, D.H. Facile Synthesis of n-type (AgIn)(x)Zn(2(1-x))S₂/p-type Ag₂S Nanocomposite for Visible Light Photocatalytic Reduction To Detoxify Hexavalent Chromium. *ACS Appl. Mater. Interfaces* **2015**, *7*, 26941–26951. [[CrossRef](#)]
116. Norseth, T. The carcinogenicity of chromium. *Environ. Health Perspect.* **1981**, *40*, 121–130. [[CrossRef](#)]
117. Zhitkovich, A. Importance of chromium-DNA adducts in mutagenicity and toxicity of chromium(VI). *Chem. Res. Toxicol.* **2005**, *18*, 3–11. [[CrossRef](#)]
118. Li, L.; Zhang, J.; Li, Y.; Yang, C. Removal of Cr(VI) with a spiral wound chitosan nanofiber membrane module via dead-end filtration. *J. Membr. Sci.* **2017**, *544*, 333–341. [[CrossRef](#)]
119. Charentanyarak, L. Heavy metals removal by chemical coagulation and precipitation. *Water Sci. Technol.* **1999**, *39*, 135–138. [[CrossRef](#)]
120. Edebali, S.; Pehlivan, E. Evaluation of Amberlite IRA96 and Dowex 1×8 ion-exchange resins for the removal of Cr(VI) from aqueous solution. *Chem. Eng. J.* **2010**, *161*, 161–166. [[CrossRef](#)]
121. Ma, H.-L.; Zhang, Y.; Hu, Q.-H.; Yan, D.; Yu, Z.-Z.; Zhai, M. Chemical reduction and removal of Cr(vi) from acidic aqueous solution by ethylenediamine-reduced graphene oxide. *J. Mater. Chem.* **2012**, *22*, 5914–5916. [[CrossRef](#)]

122. Crista, D.M.A.; Mello, G.P.C.; Shevchuk, O.; Sendao, R.M.S.; Simoes, E.F.C.; Leitao, J.M.M.; da Silva, L.P.; Esteves da Silva, J.C.G. 3-Hydroxyphenylboronic Acid-Based Carbon Dot Sensors for Fructose Sensing. *J. Fluoresc* **2019**, *29*, 265–270. [[CrossRef](#)] [[PubMed](#)]
123. Simoes, E.F.C.; da Silva, L.P.; da Silva, J.; Leitao, J.M.M. Hypochlorite fluorescence sensing by phenylboronic acid-alizarin adduct based carbon dots. *Talanta* **2020**, *208*, 120447. [[CrossRef](#)] [[PubMed](#)]
124. Crista, D.M.A.; El Mragui, A.; Algarra, M.; Esteves da Silva, J.C.G.; Luque, R.; Pinto da Silva, L. Turning Spent Coffee Grounds into Sustainable Precursors for the Fabrication of Carbon Dots. *Nanomaterials* **2020**, *10*, 1209. [[CrossRef](#)]
125. Li, J.; Tang, K.; Yu, J.; Wang, H.; Tu, M.; Wang, X. Nitrogen and chlorine co-doped carbon dots as probe for sensing and imaging in biological samples. *R. Soc. Open Sci.* **2019**, *6*, 181557. [[CrossRef](#)]
126. Zhang, H.; Huang, Y.; Hu, Z.; Tong, C.; Zhang, Z.; Hu, S. Carbon dots codoped with nitrogen and sulfur are viable fluorescent probes for chromium(VI). *Microchimica Acta* **2017**, *184*, 1547–1553. [[CrossRef](#)]
127. Zhong, Y.; Qiu, X.; Chen, D.; Li, N.; Xu, Q.; Li, H.; He, J.; Lu, J. Flexible Electrospun Carbon Nanofiber/Tin(IV) Sulfide Core/Sheath Membranes for Photocatalytically Treating Chromium(VI)-Containing Wastewater. *ACS Appl. Mater. Interfaces* **2016**, *8*, 28671–28677. [[CrossRef](#)]
128. Essner, J.B.; Kist, J.A.; Polo-Parada, L.; Baker, G.A. Artifacts and Errors Associated with the Ubiquitous Presence of Fluorescent Impurities in Carbon Nanodots. *Chem. Mater.* **2018**, *30*, 1878–1887. [[CrossRef](#)]
129. Tan, J.; Zou, R.; Zhang, J.; Li, W.; Zhang, L.; Yue, D. Large-scale synthesis of N-doped carbon quantum dots and their phosphorescence properties in a polyurethane matrix. *Nanoscale* **2016**, *8*, 4742–4747. [[CrossRef](#)]
130. Christe, S.; Esteves da Silva, J.C.G.; Pinto da Silva, L. Evaluation of the Environmental Impact and Efficiency of N-Doping Strategies in the Synthesis of Carbon Dots. *Materials* **2020**, *13*, 504. [[CrossRef](#)]
131. Fernandes, S.; Esteves da Silva, J.C.G.; Pinto da Silva, L. Comparative life cycle assessment of high-yield synthesis routes for carbon dots. *NanoImpact* **2021**, *23*, 100332. [[CrossRef](#)] [[PubMed](#)]
132. Li, L.; Lu, C.; Li, S.; Liu, S.; Wang, L.; Cai, W.; Xu, W.; Yang, X.; Liu, Y.; Zhang, R. A high-yield and versatile method for the synthesis of carbon dots for bioimaging applications. *J. Mater. Chem. B* **2017**, *5*, 1935–1942. [[CrossRef](#)] [[PubMed](#)]
133. Jing, S.; Zhao, Y.; Sun, R.-C.; Zhong, L.; Peng, X. Facile and High-Yield Synthesis of Carbon Quantum Dots from Biomass-Derived Carbons at Mild Condition. *ACS Sustain. Chem. Eng.* **2019**, *7*, 7833–7843. [[CrossRef](#)]
134. Algarra, M.; Orfãos, L.d.; Alves, C.S.; Moreno-Tost, R.; Pino-González, M.S.; Jiménez-Jiménez, J.; Rodríguez-Castellón, E.; Eliche-Quesada, D.; Castro, E.; Luque, R. Sustainable Production of Carbon Nanoparticles from Olive Pit Biomass: Understanding Proton Transfer in the Excited State on Carbon Dots. *ACS Sustain. Chem. Eng.* **2019**, *7*, 10493–10500. [[CrossRef](#)]

Disclaimer/Publisher's Note: The statements, opinions and data contained in all publications are solely those of the individual author(s) and contributor(s) and not of MDPI and/or the editor(s). MDPI and/or the editor(s) disclaim responsibility for any injury to people or property resulting from any ideas, methods, instructions or products referred to in the content.